Environmental Chemistry Letters (2022) 20:1929–1963
https://doi.org/10.1007/s10311-022-01416-x

REVIEW

Occurrence, toxicity and adsorptive removal of the chloramphenicol antibiotic in water: a review

Luan Minh Nguyen[1,2] · Ngoan Thi Thao Nguyen[1,2] · Thuy Thi Thanh Nguyen[2,3] · Thuong Thi Nguyen[1,4] · Duyen Thi Cam Nguyen[1,4] · Thuan Van Tran[1,4]

Received: 6 January 2022 / Accepted: 11 February 2022 / Published online: 25 March 2022

Abstract

Chloramphenicol is a broad-spectrum bacterial antibiotic used against conjunctivitis, meningitis, plague, cholera, and typhoid fever. As a consequence, chloramphenicol ends up polluting the aquatic environment, wastewater treatment plants, and hospital wastewaters, thus disrupting ecosystems and inducing microbial resistance. Here, we review the occurrence, toxicity, and removal of chloramphenicol with emphasis on adsorption techniques. We present the adsorption performance of adsorbents such as biochar, activated carbon, porous carbon, metal–organic framework, composites, zeolites, minerals, molecularly imprinted polymers, and multi-walled carbon nanotubes. The effect of dose, pH, temperature, initial concentration, and contact time is discussed. Adsorption is controlled by π–π interactions, donor–acceptor interactions, hydrogen bonding, and electrostatic interactions. We also discuss isotherms, kinetics, thermodynamic data, selection of eluents, desorption efficiency, and regeneration of adsorbents. Porous carbon-based adsorbents exhibit excellent adsorption capacities of 500–1240 mg g^{-1}. Most adsorbents can be reused over at least four cycles.

Keywords Chloramphenicol · Occurrence · Toxicity · Adsorption techniques · Mechanisms · Mathematic models

Introduction

Water pollution has become one of the globally major challenges over the past decades. As a result of human activities, releasing toxic compounds into water bodies exerts negative influences on aquatic ecosystems and water quality (Xu et al. 2021). These emerging pollutants include textile dyes, heavy metals, aromatic compounds, antibiotics, and other persistent organic substrates, which can be locally found in groundwater and surface water (Saravanan et al. 2021). Speaking of antibiotics, they are extensively consumed in aquaculture and frequently used in human and animal therapies. Such occurrence can, however, engender a direct discharge of antibiotic residues into water sources (Cheng et al. 2020). It was reported that antibiotic pollution over long-term disposure is a crucial factor in rising gene resistance in many bacteria (Chaturvedi et al. 2021). Many studies indicated that antibiotic pollution reduces the quality of water sources in rivers, lakes, reservoirs and irrigation systems (Li et al. 2020a, b, c, d; Xu et al. 2021).

Chloramphenicol manifests as one of emergent antibiotic pollutants (Gu et al. 2021). This compound is a broad-spectrum antibiotic isolated from the bacterium species, namely *Streptomyces venezuelae* (Roushani et al. 2020). Based on binding to the bacterial ribosomal subunit, chloramphenicol inhibits the formation of protein, causing bacterial death (Bayrakci et al. 2021). Thereby, chloramphenicol is preferable to the treatment of diseases regarding gram-positive, gram-negative, and anaerobic bacteria in humans

✉ Duyen Thi Cam Nguyen
ntcduyen@ntt.edu.vn

✉ Thuan Van Tran
tranvt@ntt.edu.vn; ttran@gradcenter.cuny.edu

[1] Institute of Environmental Technology and Sustainable Development, Nguyen Tat Thanh University, 298-300A Nguyen Tat Thanh, District 4, Ho Chi Minh City 755414, Vietnam

[2] Department of Chemical Engineering and Processing, Nong Lam University, Thu Duc District, Ho Chi Minh City 700000, Vietnam

[3] Faculty of Science, Nong Lam University, Thu Duc District, Ho Chi Minh City 700000, Vietnam

[4] NTT Hi-Tech Institute, Nguyen Tat Thanh University, 298-300A Nguyen Tat Thanh, District 4, Ho Chi Minh City 755414, Vietnam

and animals (Busch et al. 2020). With the twin advantages comprising relatively low production cost and highly stable, chloramphenicol has been widely accepted for usage in developing countries (Van et al. 2020). Indeed, this antibiotic has been found with high frequency in rivers, lakes, and seawaters as a result of livestock and aquaculture activities (Gopal et al. 2021). Therapeutic activities for humans or animals may also be responsible for the presence of chloramphenicol in hospital wastewaters (Liu et al. 2021), in the influents and effluents from wastewater treatment plants (Wang et al. 2021).

The exposure of chloramphenicol possibly causes some serious impacts on the environment and human health (Sall et al. 2020). For aquatic organisms, chloramphenicol has a high level of ecological toxicity (Zhang et al. 2021a, b, c, d). This compound inhibits the growth and development of green algae (Xiong et al. 2019), blue-green algae (Xiong et al. 2019), marine algae, and freshwater green alga (Parthasarathy et al. 2020) through specific protein control (Holanda et al. 2019). For animals, e.g., rat, cat, dog, and pig and humans, chloramphenicol is known to be a contributing factor in the aplastic anemia (Zhang et al. 2021a, b, c, d). This disease relates to deficiencies in producing red and white blood cells, leading to blood disorder, and high mortality rate (Cao et al. 2020). In addition, some researches indicated that chloramphenicol has potentially genotoxic carcinogenicity (Luo et al. 2018). Due to such negative effects, many countries such as USA, Canada, Australia, Japan, China and European Union banned the use of chloramphenicol as an additive from animal feed production (Chen et al. 2020a, b).

Considering the widespread presence and negative effects of chloramphenicol on the environment and humans, decontaminating this compound from water is a great challenge. Many approaches such as chemical (Mahdi et al. 2021), biological (Lu et al. 2020), and physicochemical methods (Yang et al. 2020a, b) have been developed to treat the pollution of chloramphenicol. In general, adsorption is one of the most widely used physicochemical methods. Indeed, this method offers many outstanding advantages such as high efficiency, reusability, flexible operation, environmental friendliness, and cost saving (Ahammad et al. 2021). In particular, adsorbent materials are very diverse, including carbon-based materials (Cheng et al. 2019), polymers (Idris et al. 2020), metal–organic frameworks (Li et al. 2020a, b, c, d), and mineral materials (Sun et al. 2017). Therefore, performance of adsorbents for the removal of chloramphenicol from wastewater should be profoundly evaluated.

To the best of our knowledge, there is currently no comprehensive review on the occurrence, toxicity, and adsorptive treatment of chloramphenicol drugs in water. Therefore, the objectives of this review are to assess the pollution, toxicity of chloramphenicol and discuss the latest results of chloramphenicol treatment performance using adsorbents in the previous studies. To better illustrate, Fig. 1 manifests the main sources and mitigation of chloramphenicol antibiotic from water. This study is organized by the following main sections: (i) occurrence and pollution of chloramphenicol in the aquatic environment, wastewater treatment plants, hospital wastewater; (ii) assessment of toxicity of chloramphenicol exposure in humans and animals; (iii) treatment of chloramphenicol with an emphasis on adsorption technique. The selection of adsorption as a major treatment method is also explained. The performance of various adsorbents such as biochars, activated carbons, porous carbons, metal–organic frameworks, composites, molecularly imprinted polymers, and other adsorbents is systematically mentioned. Here, we evaluate several parameters affecting the efficiency of

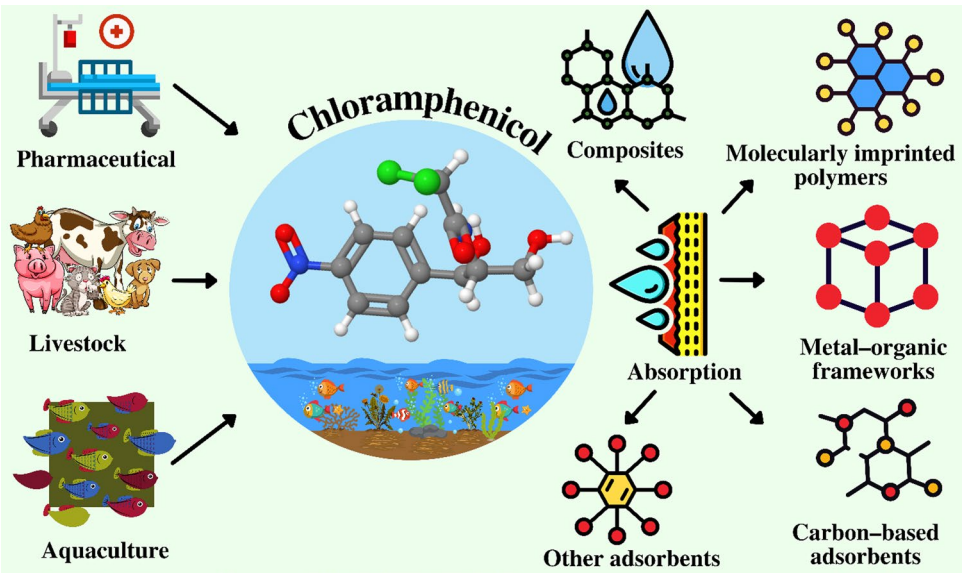

Fig. 1 Sources and mitigation of the chloramphenicol antibiotic in water. To attenuate the pollution of chloramphenicol, adsorption is used as an effective, flexible and high-performance technique. Advanced adsorbents including nanocomposites, metal–organic frameworks, molecularly imprinted polymers, and carbon-based nanomaterials have been recently developed to deal with chloramphenicol pollution

chloramphenicol removal as well as to elucidate the plausible mechanisms controlling the chloramphenicol adsorption. Kinetic, isotherm, thermodynamic models are mentioned in this study. Some limitations and prospects of chloramphenicol adsorption in aqueous medium are suggested to orientate further studies.

Occurrence and pollution

Aquatic environment

Main pollution sources of chloramphenicol comprise aquaculture, hospital wastewaters, therapeutic activities for human and livestock, pharmaceutical production as illustrated in Fig. 2. In the aquatic environment, the occurrence and distribution of chloramphenicol pollution can be recorded in surface water, river, groundwater, and sea (Table 1). Accordingly, many rivers around the world daily receive a certain amount of chloramphenicol from human and aquafarming activities. Indeed, Lin et al. (2008) reported that household wastewater containing a very low chloramphenicol concentration of 1 ng L^{-1} was discharged into rivers in Taiwan. Choi et al. (2008) revealed a higher average level of chloramphenicol of 31 ng L^{-1} found in the mainstream of the Han River, Korea. At the same trend, Lu et al. (2009) investigated the chloramphenicol concentration up to 112.3 ng L^{-1} in the aquaculture farms in Guangzhou, China. Oluwatosin et al. (2016) evaluated the presence of this drug in the surface water with a maximum concentration of 360 ng L^{-1} in Lagos, Nigeria. In Malaysia, chloramphenicol levels were found to be the highest in the Selangor River of 24.35 ng L^{-1}, followed by the Gombak River of 23.37 ng L^{-1}, and finally the Lui River of 18.03 ng L^{-1} (Praveena et al. 2018). In another study, Jiang et al. (2011) compared the difference in chloramphenicol residues between two rivers in China. Specifically, Pearl River had a significantly higher concentration of chloramphenicol, of 266 ng L^{-1}, than Huangpu River, of 28.36 ng L^{-1}.

The presence of chloramphenicol in urban lakes and canals has been also recorded (Tran et al. 2019a, b, c). This might be because the rivers that contaminated a large amount of chloramphenicol flow directly into lakes and canals. As a result, these drainage systems are affected by chloramphenicol pollution. For example, Tran et al. (2019a, b, c) found a wide range of chloramphenicol concentrations of 18–155 ng L^{-1} in West Lake, Hoan Kiem Lake, Yen So Lake, To Lich Canal, and Kim Nguu Canal in Hanoi, Vietnam. Similarly, Zhou et al. (2019) showed that chloramphenicol at an average level of 4.89 ng L^{-1} existed in shallow lakes in the Yangtze River basin, China. More surprisingly, Tahrani et al. (2016) collected the seawater samples in Herglas Sea, Tunisia, and found that the highest concentration of chloramphenicol was 15,600 ng L^{-1}.

The detection of chloramphenicol from river water samples is widely varied by season. Liu et al. (2009) pointed out Nanming River in the winter displayed a notably higher chloramphenicol threshold than that in the summer. Specifically, the mean level of chloramphenicol in the downstream was 11,200 ng L^{-1} in the winter, compared with 1300 ng L^{-1} in the summer. Kong et al. (2014)

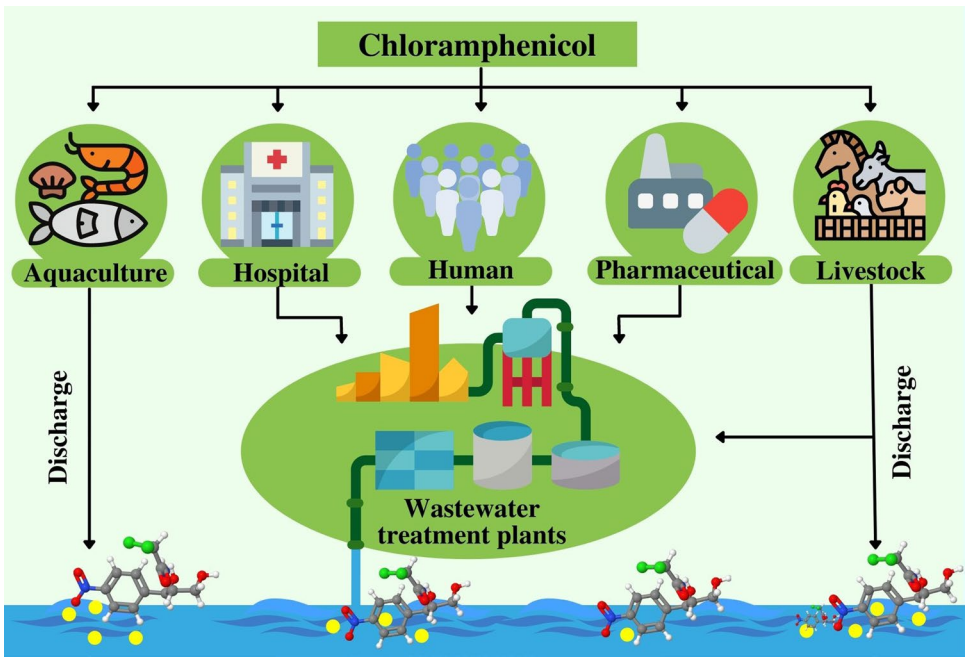

Fig. 2 Main pollution sources of chloramphenicol comprise aquaculture, hospital wastewaters, therapeutic activities for humans and livestock, pharmaceutical production. Aquaculture activities directly discharge chloramphenicol into water. The others are treated by wastewater treatment plants, but chloramphenicol residue still exists in the effluents

Table 1 Occurrence of chloramphenicol in the aquatic environment

Location	Source	Chloramphenicol concentration	References
Pearl River Guangzhou, China	River water	11–266 ng L^{-1} in the high water season 54–187 ng L^{-1} in the low water	Xu et al. (2007)
Nanming River, Guiyang, China	River water	600 ng L^{-1} in the upstream waters 11,200 ng L^{-1} in the downstream waters	Liu et al. (2009)
Guangzhou, China	Surface water	112.3 ng L^{-1} in freshwater aquaculture pond	Lu et al. (2009)
Huangpu River, Shanghai, China	Surface water	28.36 ng L^{-1} in center of the stream	Jiang et al. (2011)
Yangtze River basin, China	Surface water	4.89 ng L^{-1} in shallow lakes	Zhou et al. (2019)
Taiwan	River water	1 ng L^{-1} in household wastewaters	Lin et al. (2008)
Seoul, Korea	Surface water	31 ng L^{-1} in Han River	Choi et al. (2008)
Grand-Tunis, Tunisia	Sea water	400 ng L^{-1} in Tunis	Tahrani et al. (2016)
Grand-Tunis, Tunisia	Sea water	3500 ng L^{-1} in Monastir	Tahrani et al. (2016)
Grand-Tunis, Tunisia	Sea water	15,600 ng L^{-1} in Hergla	Tahrani et al. (2016)
Grand-Tunis, Tunisia	Sea water	200 ng L^{-1} in Sousse	Tahrani et al. (2016)
Hanoi, Vietnam	Surface water	22 ng L^{-1} in West Lake	Tran et al. (2019a, b, c)
Hanoi, Vietnam	Surface water	19 ng L^{-1} in Hoan Kiem Lake	Tran et al. (2019a, b, c)
Hanoi, Vietnam	Surface water	18 ng L^{-1} in Yen So Lake	Tran et al. (2019a, b, c)
Hanoi, Vietnam	Surface water	155 ng L^{-1} in To Lich Canal	Tran et al. (2019a, b, c)
Hanoi, Vietnam	Surface water	137 ng L^{-1} in Kim Nguu Canal	Tran et al. (2019a, b, c)
Selangor, Malaysia	Surface water	15.8–18.03 ng L^{-1} in the Lui River	Praveena et al. (2018)
Selangor, Malaysia	Surface water	22.72–23.37 ng L^{-1} in the Gombak River	Praveena et al. (2018)
Selangor, Malaysia	Surface water	21.48–24.35 ng L^{-1} in the Selangor River	Praveena et al. (2018)
Kisat River, Kenya	River water	20 ± 50 ng L^{-1} in the upstream waters 60 ± 80 ng L^{-1} in the downstream waters	Kimosop et al. (2016)
Lagos, Nigeria	Surface water	360 ng L^{-1} in Owo River	Oluwatosin et al. (2016)

interpreted that high temperature of water in the summer strongly affected the decomposition rate of chloramphenicol in the rivers. Consequently, the chloramphenicol concentration in rivers in hot seasons may be lower than that in cold seasons. On the other hand, Xu et al. (2007) indicated that there was a slight disparity of chloramphenicol concentrations in Pearl River in the high and low water seasons in range of 11–266 ng L^{-1}, and 54–187 ng L^{-1}, respectively. This difference could be attributable to the flow of water, which means that water flow was larger in high water seasons, and vice versa. During the high water season, aquaculture activities flourished in the rivers, leading to a remarkable increase in the presence of chloramphenicol through disease treatments and feedings (Huys et al. 2007). Moreover, the concentration of chloramphenicol would be more diluted during the high water season, and hence, the variation of the chloramphenicol concentration became wider. Although the use of chloramphenicol in aquaculture activities has been restricted, this antibiotic still exists and accumulates in the rivers, lakes, and seas with high frequency. Controlling the consumption of chloramphenicol for livestock and aquaculture activities is highly recommended.

Wastewater treatment plants

Wastewater treatment plants are the places that receive and treat the polluted water from the major sources involving sewages, domestic wastewaters, industrial wastewaters, and a part of agricultural wastewaters (Table 2). Therefore, many ecological contaminants including chloramphenicol can be also present in the influents and effluents of wastewater treatment plants. Indeed, Sui et al. (2011) measured the presence of chloramphenicol in the influent up to 71.9 ng L^{-1} and effluent up to 46.9 ng L^{-1} in the municipal wastewater treatment plants in Beijing, China. Tahrani et al. (2016) monitored the level of chloramphenicol in two various regions in Tunisia. The results indicated that the influent and effluent in Tunis-nord wastewater treatment plants exhibited chloramphenicol concentrations of 3.3, and 1.1 ng mL^{-1}, while those in Chotrana were 500 and 300 ng L^{-1}, respectively. This could be the difference of treatment technologies at these two wastewater treatment plants which consisted of the pretreatment, primarily settling, and biological methods. Likewise, Barbara et al. (2009) compared the amount of chloramphenicol in the inlet wastewater of two municipal wastewater treatment plants in South Wales, the UK. According to the measured results, the influent of wastewater

Table 2 Occurrence of chloramphenicol in wastewater treatment plants

Location	Source	Concentration		References
		In the influent	In the effluent	
Guangzhou, China	Industrial and residential wastewater	1730–2430 ng L^{-1}	Not detected–1460 ng L^{-1}	Peng et al. (2006)
Beijing, China	Municipal sewage	29[a] ng L^{-1}	19 ng L^{-1}	Sui et al. (2010)
Beijing, China	Municipal sewage	not detected–71.9 ng L^{-1}	not detected–46.9 ng L^{-1}	Sui et al. (2011)
Victoria Harbor, Hong Kong	Stonecutters Island	–	234 ng L^{-1}	Minh et al. (2009)
Victoria Harbor, Hong Kong	Tai Po	–	15.5 ng L^{-1}	Minh et al. (2009)
Victoria Harbor, Hong Kong	Central	–	364 ng L^{-1}	Minh et al. (2009)
Victoria Harbor, Hong Kong	Wan Chai East	–	265 ng L^{-1}	Minh et al. (2009)
Victoria Harbor, Hong Kong	Wan Chai West	–	613 ng L^{-1}	Minh et al. (2009)
Victoria Harbor, Hong Kong	North Point	–	100 ng L^{-1}	Minh et al. (2009)
Singapore	Municipal sewage	62–80 ng L^{-1}	1.5 [a] ng L^{-1}	Tran et al. (2016)
Grand-Tunis, Tunisia	Tunis-nord	3300 ng L^{-1}	1100 ng L^{-1}	Tahrani et al. (2016)
Grand-Tunis, Tunisia	Chotrana	500 ng L^{-1}	300 ng L^{-1}	Tahrani et al. (2016)
South Wales, United Kingdom	Coslech	150–452 ng L^{-1}	6[a] –69 ng L^{-1}	Kasprzyk-Hordern et al. (2009)
South Wales, United Kingdom	Cilfynydd	4[a] –319 ng L^{-1}	6[a] ng L^{-1}	Kasprzyk-Hordern et al. (2009)

[a]Data estimated from the figures of the referred study

treatment plants in Coslech had a higher concentration of chloramphenicol, of 150–452 ng L^{-1}, than Cilfynydd, of 4–319 ng L^{-1}. In another study, Peng et al. (2006) demonstrated the treatment performance of wastewater treatment plants was profoundly dependent on the influent wastewater sources in Guangzhou, China. Specifically, the removal of chloramphenicol in industrial wastewater was greatly difficult than domestic wastewater. The principal reason relies on the co-existence of various industrial pollutants, particularly in textile dyes and heavy metals with very high concentrations. Peng et al. (2006) also explained that the industrial wastewaters majorly stemmed from food, chemical, and pharmaceutical industries. As a result, most wastewater treatment plants incompletely treated chloramphenicol from the wastewaters.

A considerable amount of chloramphenicol after the treatment process in wastewater treatment plants was recorded in many previous studies. In Hong Kong, Minh et al. (2009) reported that although wastewater treatment plants applied many chemical and physical methods to remove chloramphenicol from the wastewaters, the removal efficiency was generally not satisfactory. Consequently, Victoria Harbor in Hong Kong has received record-high levels of chloramphenicol from the Stonecutters Island of 234 ng L^{-1}, Tai Po of 15.5 ng L^{-1}, Central of 364 ng L^{-1}, Wan Chai East of 265 ng L^{-1}, Wan Chai West of 613 ng L^{-1}, and North Point of 100 ng L^{-1} (Minh et al. 2009). At the same trend, Sui et al. (2010) revealed that chloramphenicol was not completely eliminated in the secondary effluent in Beijing, China. By contrast, Tran et al. (2016) detected a very low content, less than 1.5 ng L^{-1} of chloramphenicol from wastewater samples treated by wastewater treatment plants in Singapore. This result was tightly related to the low levels of chloramphenicol in raw influents (Kasprzyk-Hordern et al. 2009). Tong et al. (2009) and Tran et al. (2016) interpreted that the policies of banning chloramphenicol usage in livestock breeding in many countries including Singapore and China lowered the level of chloramphenicol in wastewater. To sum up, there are large disparities in the chloramphenicol concentration among wastewater treatment plants, which reflects the importance of treatment technologies.

Hospital wastewaters

In recent years, chloramphenicol use for therapeutic activities has been significantly restrained in several hospitals due to its side effects such as aplastic anemia (Rich et al. 1950) and bone marrow suppression (Ambekar et al. 2000). Although the presence of chloramphenicol in hospital wastewaters is less mentioned, it is still necessary to discuss systematically. Lin et al. (2008) showed a low level of chloramphenicol, less than 1 ng L^{-1} in the effluent from hospitals in Taiwan. Meanwhile, Kimosop et al. (2016) conducted a thorough investigation of wastewater samples from the hospitals in Kakamega, Mumias, Bungoma, and Eldoret in Lake Victoria Basin, Kenya. The monitoring techniques confirmed that the concentration of chloramphenicol in the hospital wastewater effluent was in range from 60 ng L^{-1} to 100 ng L^{-1}. This study alarmed a serious discharge of chloramphenicol in hospital wastewaters in Kenya. Summarily, there has a marked contrast of chloramphenicol concentration detected in the hospital wastewater effluents between

two countries. It can be surmised that the law regulations play a vital role in controlling chloramphenicol use in hospitals and indirectly prevent the presence of this drug in the wastewaters.

Toxicity

In this section, the ecological toxicity and negative effects of chloramphenicol on aquatic environments, animals, and humans are discussed as illustrated in Fig. 3. The pollution of chloramphenicol drugs in water originates from hospital effluents, veterinary husbandry wastewater, and aquafarming. Untreated wastewater containing chloramphenicol is directly discharged into the aquatic environment, causing the influence of aquaculture, livestock, domestic water quality (Lulijwa et al. 2020). A high concentration of chloramphenicol in water can inhibit the growth of aquatic organisms, damage cells and change the biochemical properties of water (Yunis 1989). Table 3 summarizes some negative effects of chloramphenicol on various living objects involving humans, female mice, Wistar rats, cats, dogs, pigs, and algae.

Algae species are predominantly aquatic organisms, and they play a critical role in maintaining the balance of the aquatic ecosystems (Lai et al. 2009; Stevenson 2014). Many works pointed out the effect of chloramphenicol on algae species (Leston et al. 2013; Xiong et al. 2019). Indeed, Xiong et al. (2019) reported that chloramphenicol was likely to inhibit the synthesis of fatty acid, increasing the possibility of protein and deoxyribonucleic acid aggregation. This fact resulted in the increasing accumulation of lipid-peroxidative products, thereby causing a substantial loss of β-sheet protein of β-sheet protein. At the same trend, Leston et al. (2013) found the uptake and accumulation of the chloramphenicol drug and its profound effects on the growth of green macroalgae *Ulva lactuca*. Campa et al. (2006) indicated that chloramphenicol was less likely to affect the *Isochrysis galbana* species at low concentration of less than 12 mg L^{-1}. Compared with this study, Lai et al. (2009) found that chloramphenicol could only prevent the growth of the same algae species at concentrations higher than 20 mg L^{-1}. This difference may be due to the experimental conditions such as light, temperature, and salinity between these works which the *Isochrysis galbana* species were grown.

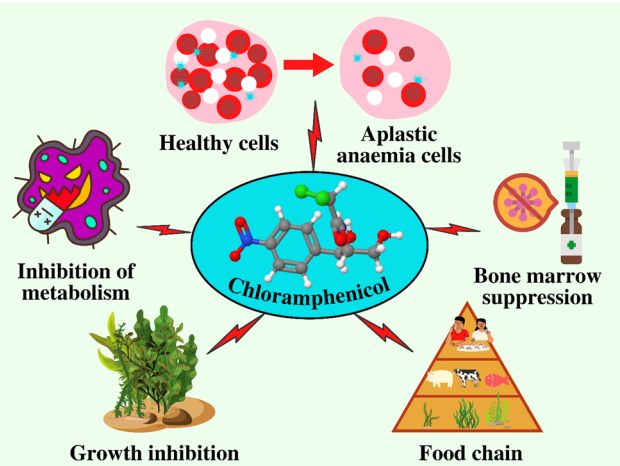

Fig. 3 Toxicity and effects of chloramphenicol on human health and the environment. For humans, aplastic anemia and bone marrow suppression are attributable to the side effects of chloramphenicol. Aplastic anemia leaves the human body more vulnerable, and uncontrolled bleeding, as well as prone to infections. For aquatic organisms, chloramphenicol inhibits the synthesis of fatty acid, increases the possibility of protein and deoxyribonucleic acid aggregation, and accumulation of lipid-peroxidative products, causing a substantial loss of β-sheet protein. As a result, this compound adversely affects the growth and metabolism of algae species as well as other aquatic organisms, unbalancing the aquatic ecosystems and food chains

Likewise, microalgae are one of the important microorganisms of the food chain. Kaparapu (2018) assessed the importance of microalgae as food sources for many aquatic animals such as fish and shrimp. Moreover, some soft-bodied creatures such as bivalve mollusks, e.g., oysters, scallops, and larval stages of abalone would be benefited from microalgae species. When antibiotics such as chloramphenicol accumulate in microalgae, the aquatic species, e.g., fish and shrimp can be directly accumulated with toxins through this food chain (Lu et al. 2009). Consequently, human health can be endangered by the consumption of chloramphenicol-contaminated food sources.

Some medicines containing chloramphenicol as one of their ingredients can cause many potent side effects on patient health. Previous works reported the harmful effects of chloramphenicol in inhibiting the metabolism or reducing the effectiveness of some drugs, e.g., tolbutamide, and penicillin in the treatment of human diseases (Christensen and Skovsted 1969; Koup et al. 1978). Moreover, some diseases such as aplastic anemia (Rich et al. 1950) and bone marrow suppression (Ambekar et al. 2000) are attributable to the side effects of chloramphenicol. Aplastic anemia is a rare, dose independent, irreversible, idiosyncratic manifestation (Shukla et al. 2011). This pharmaceutical damages the stem cells produced by bone marrow, stopping generating new blood cells. Hence, the human body is more vulnerable, and prone to infections as well as uncontrolled bleeding. Many countries such as the USA, European Union, and Canada have limited the use of chloramphenicol for animal and human therapies (Samsonova et al. 2012; Yanovych et al. 2018). However, Samsonova et al. (2012) pointed out that chloramphenicol is still being used in some developing countries for the purposes of aquaculture. In fact, chloramphenicol has many notable advantages such as high efficiency, good antibacterial activity, and low cost in the treatment

Table 3 Effect of chloramphenicol on various living organisms

Organism	Possible effects	References
Human (12-year-old patient)	Inhibit mitochondrial protein synthesis	Wiest et al. (2012)
Human	Causes optic disk congestion with blurred margins, swelling of polymer modified bitumen, and central fibroids leading to optic neuropathy	Wang and Sadun (2013)
Human	Nitrobenzene metabolites of the chloramphenicol impact on the deoxyribonucleic acid lead to aplastic anemia in humans	Ohnishi et al. (2015)
Human (neonates and infants lacking glucuronidation reactions)	Prolonged use of chloramphenicol can cause gray syndrome (low blood pressure, heart failure, gray skin)	McIntyre and Choonara (2004)
Female mice	Inhibits protein synthesis in the mitochondria of myeloid progenitor cells in the doses of chloramphenicol at 2500 and 3500 mg kg^{-1} for 5 days	Turton et al. (2006)
Wistar rats	Causes blood vessel congestion Appearance of foam in the cytoplasm of hepatocytes in the central region of the liver (hitopathology)	Saba et al. (2016)
Cattle	Capable of causing diarrhea or inappetence	Dowling (2013)
Cats	Causes a decrease in the number of white blood cells and the percentage of red blood cells in the blood (50 mg kg^{-1} body weight in 21 days) Causes severe depression	Penny et al. (1967)
Dogs	Decreased mitotic activity and reduced rate of granulocytopoiesis (275 mg kg^{-1} body weight/day in 14 days) Inhibits erythropoiesis in the bone marrow	Watson (1977)
Pigs	Chloramphenicol causes hepatotoxicity, neurotoxicity and disturbed intestinal epithelium (20 mg kg^{-1} body weight, twice every 24 h)	Klebaniuk et al. (2018)
Green macroalgae: *Ulva lactuca*	Chloramphenicol is accumulated and transferred along the trophic web in *Ulva lactuca* in higher levels	Leston et al. (2013)
Green algae: *Pseudokirchneriella subcapitata, Scenedesmus quadricauda, Scenedesmus obliquus, Scenedesmus acuminatus*	Inhibit the synthesis of fatty acid Increase the possibility of protein and deoxyribonucleic acid aggregation	Xiong et al. (2019)
Blue-green alga: *Aegilops cylindrica*	Inhibit the production of cyanophycin granule polypeptide	Simon (1973)
Freshwater green alga: *Chlorella pyrenoidosa*	Half-maximal effective concentration of 14 mg L^{-1}	Lai et al. (2009)
Marine algae: *Isochrysis galbana*, *Tetraselmis chui*	Half-maximal effective concentration of 4–41 mg L^{-1}	Lai et al. (2009)
Alga: *Chaetoceros gracilis*	Chloramphenicol at a dose of 3.0 mg L^{-1} significantly sensitized the algae *Chaetoceros gracilis*	Campa et al. (2006)

and prevention of infectious diseases in animals. To sum up, a serious consideration for the use of chloramphenicol is required to alleviate the possible effects on aquatic environments, animals, and humans.

Removal of chloramphenicol

Selection of treatment methods

There are many methods, e.g., physical, chemical, and biological for the treatment of chloramphenicol in aqueous media. For example, the chemical methods use the advanced oxidation process to degrade this antibiotic (Mahdi et al. 2021). The reagents of the advanced oxidation process are strong oxidants, e.g., H_2O_2, persulfate, and ozone to mineralize or oxidize organic pollutants into simple compounds such as CO_2, H_2O, and N_2 (Wang and Zhuan 2020). However, the chemical methods have many chief disadvantages, e.g., toxic oxidants, ultraviolet radiation, expensive chemicals, and high cost (Cuerda et al. 2020). Meanwhile, the biological methods take advantage of microorganisms to eliminate antibiotics under aerobic and anaerobic conditions (Oberoi et al. 2019). The plants can also degrade antibiotic compounds through the phytoremediation process. Microorganisms undertake nitrogen fixation from the structure of chloramphenicol as a nutrient source for growth (Xu et al. 2019). Two downsides of the biological methods are low removal efficiency,

and long treatment duration (Lu et al. 2020). By contrast, the physicochemical methods, specifically adsorption, have proved as the most reasonable choice for the treatment of antibiotic pollutants (Balarak et al. 2020). The adsorption processes have many significant advantages including high efficiency, reusable adsorbents, easy operation, environmental friendliness, and cost savings (Shi et al. 2020). This chapter will, therefore, discuss the treatment of chloramphenicol in water using adsorption techniques.

Performance of adsorbents

Biochar

According to Table 4, the biochar-based adsorbents have been widely applied for the removal of chloramphenicol. The most important reason for this situation may be the low production cost of biochars. Most of them are produced from the pyrolysis of agricultural biomass wastes in the absence or deficiency of oxygen (Dai et al. 2019). Also, biochar materials have high hydrophobicity, offering a good compatibility with hydrophobic structure of chloramphenicol (Tong et al. 2019). The pyrolysis temperature of the biomass significantly influences on the properties and adsorption efficiency of obtained biochars. Indeed, Yang et al. (2020a, b) proved that rice straw biochar pyrolyzed at 700 °C, N_2 flow reached a higher chloramphenicol adsorption efficiency than biochars pyrolyzed at 350 °C or 500 °C. On the other hand, biochars expose their inherent weaknesses of poor surface chemistry and low surface area. This means that a large amount of biochars is required for chloramphenicol adsorption, and scalability would be a huge challenge. To settle such drawbacks, scientists have developed novel functionalized biochars (Cheng et al. 2021). For example, Fan et al. (2010) demonstrated that bamboo biochars treated with NaOH considerably boosted the surface functional groups. As a result, chloramphenicol adsorption efficiency by modified biochars was approximately four times higher than unmodified biochars. Ahmed et al. (2017a) showed that chloramphenicol was almost eliminated from water using biochars treated by 50% H_3PO_4. To sum up, functionalization of biochars is necessary to improve chloramphenicol removal, but negative effects of residual chemical modifiers on the environment should be also considered.

Activated carbon

Activated carbons are highly porous materials constituted of sp^2-hybrized carbon atoms in their network. As same as biochars, they can directly be produced from biomass (Xiang et al. 2019). Activated carbons not only surmount the inherent weaknesses but also inherit good characteristics of biochars by creating new pores, and high porosity through activation (Ouyang et al. 2020). For instance, activated carbon from coconut shell achieved a specific surface area of 1108.4 $m^2\ g^{-1}$, and pore volume of 0.4323 $cm^3\ g^{-1}$, approximately 2 times larger than wood biochar (Herath et al. 2019). Lach (2019) demonstrated that pores and surface area of activated carbons are directly proportional to their adsorption performance. Indeed, they found activated carbon with the largest specific surface of 1692 $m^2\ g^{-1}$, and pore volume of 2.103 $cm^3\ g^{-1}$ exhibited the highest chloramphenicol adsorption capacity of 214.91 mg g^{-1}.

In addition, chemical activators can substantially improve the porosity of activated carbons, leading to an enhancement of removal efficiency of chloramphenicol. Specifically, Li et al. (2018) demonstrated that activation by phosphoric acid increased the number of acidic oxygenated functional groups of activated carbon produced from *Typha orientalis*. These oxygenated groups act as hydrogen bonding donor and acceptor sites, which participated in the formation of adsorbent–adsorbate interactions. Chitongo et al. (2019) showed that carbons from grape slurry waste activated by KOH instead of HCl gave the efficiency increased by 20%. These encouraging results contribute greatly to dealing with the alarming problem of antibiotic contamination in developing countries.

Porous carbon

Among the advanced materials, porous carbons possess a variety of outstanding properties such as high surface area, large pore, surface chemistry, and high porosity. To synthesize porous carbons, precursors can be selected from elementary sources, e.g., petroleum cokes, bovine bone, fallen leaves, and chicken feathers to advanced sources, e.g., metal–organic framework, zeolitic imidazolate frameworks, and functionalized polymers. For example, hierarchical porous carbon from bovine bone obtained a surprisingly high surface area of 3231.8 $m^2\ g^{-1}$ and total pore volume of 1.976 $cm^3\ g^{-1}$ (Dai et al. 2018a). This porous carbon reached an equilibrium chloramphenicol adsorption of 1240 mg g^{-1} at 45 °C. Tran et al. (2019a, b, c) demonstrated a significant increase in specific surface area and pore volume of mesoporous carbon from metal–organic framework $Fe_3O(BDC)_3$, BDC: benzene-1,4-dicarboxylate, pyrolyzed at 700 °C in comparison with its $Fe_3O(BDC)_3$ precursor. Adhered by this trend, the adsorption capacity of $Fe_3O(BDC)_3$-derived mesoporous carbon was determined at 96.3 mg/g, compared with 24.1 mg/g of $Fe_3O(BDC)_3$.

Notably, porous carbons acquired a high diversity of structural pores such as micropores with pore size lower than 2 nm, mesopores with pore size between 2 and 50 nm, and macropores with pore size lower than 50 nm (Wang et al. 2020). Porous carbons with micro-sizes or meso-sizes may be conducive for the adsorption of small

Table 4 Chloramphenicol adsorption performance of various adsorbents

Adsorbents	pH	C_o (mg L^{-1})	Time (min)	Tem. (°C)	Dose (g L^{-1})	Q_m (mg g^{-1})	RE (%)	References
Biochars								
Biochars pyrolyzed at 350 °C	7	40	1080	25	0.5	10	–	Yang et al. (2020a, b)
Biochars pyrolyzed at 500 °C	7	40	1080	25	0.5	14.2	–	Yang et al. (2020a, b)
Biochars pyrolyzed at 700 °C	7	40	1080	25	0.5	33	–	Yang et al. (2020a, b)
Mixed HCl/HF-modified biochars pyrolyzed at 350 °C	7	40	2160	25	0.5	11.5	–	Yang et al. (2020a, b)
Mixed HCl/HF-modified biochars pyrolyzed at 500 °C	7	40	2160	25	0.5	14.7	–	Yang et al. (2020a, b)
Mixed HCl/HF-modified biochars pyrolyzed at 700 °C	7	40	2160	25	0.5	60.2	–	Yang et al. (2020a, b)
Bamboo charcoal-based biochar	4–4.5	0.25–50	2400	25	100	8.46	–	Ahmed et al. (2017b)
Bamboo charcoal-based biochar	7	30	24	30	1	8.1	–	Liao et al. (2013)
Bamboo charcoal-based biochar	–	20	15	25	8	0.65	–	Fan et al. (2010)
Sodium hydroxide-modified bamboo charcoal	–	20	15	25	8	2.35	–	Fan et al. (2010)
Peanut shell-based porous biochar	7 [a]	300	1440	40	1	423.7	90 [a]	Yang et al. (2020a, b)
Functionalized biochar								
H_3PO_4-activated biochar at 600 °C	4–4.5	0.25–50	2400	25	50–60	64.79	–	Ahmed et al. (2017b)
H_3PO_4-activated biochar at 600 °C	4–4.5	0.25–50	2400	25	50–60	75.29	–	Ahmed et al. (2017b)
H_3PO_4-activated biochar at 600 °C	4.0–4.25	0.25–20	1800	25	80	21.35	–	Ahmed et al. (2017a)
Activated carbon								
KOH-activated carbon	–	150	120	50	0.02	256.41	–	Wu et al. (2018)
Commercial activated carbon (F–300)	7	484.70	120	20	4	0.099	94.7	Lach and Kubicka (2017)
Commercial activated carbon (ROW 08 Supra)	2	484.70	120	40	4	0.12	94.7	Lach and Kubicka (2017)
Commercial activated carbon (WG–12)	2	484.70	120	60	4	0.114	93.3	Lach and Kubicka (2017)
HCl-activated grape slurry waste	7	30	90	25	16	1.71	72,69	Chitongo et al. (2019)
KOH-activated grape slurry waste	7	30	150	25	16	2.55	91.08	Chitongo et al. (2019)
Commercial activated carbon (F–300)	2	161	480	20	4	200,67	–	Lach (2019)
Commercial activated carbon (F–100)	2	161	600	20	4	174,68	–	Lach (2019)
Commercial activated carbon (WG–12)	2	161	600	20	4	195.45	–	Lach (2019)
Commercial activated carbon (ROW 08 Supra)	2	161	600	20	4	212.29	–	Lach (2019)
Commercial activated carbon (Picabiol)	2	161	360	20	4	214.91	–	Lach (2019)

Table 4 (continued)

Adsorbents	pH	C_o (mg L^{-1})	Time (min)	Tem. (°C)	Dose (g L^{-1})	Q_m (mg g^{-1})	RE (%)	References
Activated carbon pyrolyzed at 800 °C	2	161	360	20	4	343.12	–	Lach (2019)
Enteromorpha prolifera-based activated carbon	–	400–1000	240	20	0.5	709.2	–	Zhu et al. (2017)
Typha orientalis-based activated carbon	6.2	65	360	25	0.6	137.1	87.8	Li et al. (2018)
Commercial powdered activated carbon	–	100	360	25	1	304.878	90	Zhang et al. (2021a, b, c, d)
Corn stover-based activated carbon	7	25	120	25	8	32.3	100 [a]	Cheng et al. (2019)
Metal–organic frameworks								
$Fe_3O(BDC)_3$	4	10	60	25	0.4	24.10	25,60 [a]	Tran et al. (2019a, b, c)
PCN–222(Zr)	6.3	500	1 [a]	25	1	370	99 [a]	Zhao et al. (2018)
MIL–53(Al)	–	50	180	25	0.2	104.7 [a]	–	Li et al. (2020a, b, c, d)
ZIF–8	–	50	180	25	0.2	23.9 [a]	–	Li et al. (2020a, b, c, d)
UiO-66–NH_2	–	50	180	25	0.2	34.2 [a]	–	Li et al. (2020a, b, c, d)
NH_2–MIL–125(Ti)	–	50	180	25	0.2	66.4 [a]	–	Li et al. (2020a, b, c, d)
Polymers								
Functional monomer methacrylic acid–molecularly imprinted polymers	8	100	80	25	5	68.03	–	Idris et al. (2020)
Functional monomer methacrylic acid–non-imprinted polymers	8	100	180	25	5	62.5	–	Idris et al. (2020)
Silica core–shell imprinted polymer	8	100	80	25	5	32.26	–	Idris et al. (2020)
Silica core–shell non-imprinted polymers	8	100	180	25	5	29.59	–	Idris et al. (2020)
Core–shell molecularly imprinted polymers based on magnetic chitosan	–	48.47	60	25	0.5	17.32	–	Ma et al. (2015)
Core–shell molecularly non-imprinted polymers based on magnetic chitosan	–	48.47	60	25	0.5	11.18	–	Ma et al. (2015)
Core–shell surface imprinted nanospheres–magnetic mesoporous nanosilica	–	32.31	30	25	0.5	403.92	–	Dai et al. (2016)
Core–shell surface non-imprinted nanospheres–magnetic mesoporous nanosilica	–	32.31	60	25	0.5	359	–	Dai et al. (2016)
Chitosan-based molecularly imprinted polymers	–	800	40	25	15	32	–	Wang et al. (2014)
Chitosan-based non-molecularly imprinted polymers	–	800	60	25	15	6	–	Wang et al. (2014
Porous molecularly imprinted polymer halloysite nanotube	–	32.31	80	25	0.5	79.39	–	Ma et al. (2020)
Porous molecularly non-imprinted polymer halloysite nanotube	–	32.31	80	25	0.5	29.54	–	Ma et al. (2020)

Table 4 (continued)

Adsorbents	pH	C_o (mg L^{-1})	Time (min)	Tem. (°C)	Dose (g L^{-1})	Q_m (mg g^{-1})	RE (%)	References
Composite								
Fe_3O_4-supported bovine serum albumin	–	0.2	50	25	2	147.83	96.4	Zhang et al. (2013)
Fe_3O_4-functionalized biochar	4.0–4.5	1	1080 [a]	25	0.5	83.67 [a]	100	Ahmed et al. (2017a, b, c)
Nanoscale zero-valent iron supported functionalized biochar	4.0–4.5	1	720–900 [a]	25	0.5	131.44 [a]	100	Ahmed et al. (2017a, b, c)
Activated carbon-supported nanoscale zero-valent iron	7	96.94	30	30	0.2	–	67 [a]	Xu et al. (2020)
Multi-walled carbon nanotubes-supported nanoscale zero-valent iron	7	96.94	30	30	0.2	–	100 [a]	Xu et al. (2020)
Carbon powder-supported nanoscale zero-valent iron	7	96.94	30	30	0.2	3000	100 [a]	Xu et al. (2020)
Biochar supported nanoscale zero-valent iron	7	96.94	30	30	0.2	–	97 [a]	Xu et al. (2020)
Graphene oxide supported nanoscale zero-valent iron	7	96.94	30	30	0.2	–	100 [a]	Xu et al. (2020)
Nanoscale zero-valent iron particles supported activated carbon	–	150	120	50	0.02	1563.97	–	Wu et al. (2018)
Porous carbon								
$Cu_3(BTC)_2$-derived porous carbon at 700 °C	6.9	5	120	25	0.56	37.2	87.6	Tran et al. (2019a, b, c)
Potassium citrate-activated porous carbons at 900 °C	9	150	250	25	0.2	588.24	–	Dai et al. (2018c)
Porous carbons from potassium citrate pyrolyzed at 750 °C	11	300	300	25	0.2	394.9	–	Tian et al. (2017)
Potassium citrate-activated porous carbons at 800 °C	11	300	300	25	0.2	451.3	–	Tian et al. (2017)
Potassium citrate-activated porous carbons at 850 °C	11	300	300	25	0.2	506.1	–	Tian et al. (2017)
Potassium citrate-activated porous carbons at 900 °C	11	300	300	25	0.2	467.50	–	Tian et al. (2017)
Porous carbon pyrolyzed at 750 °C	4	120	420	30	0.15	480.5	–	Chen et al. (2021)
Porous carbon pyrolyzed at 800 °C	4	120	420	30	0.15	531.8	–	Chen et al. (2021)
Porous carbon pyrolyzed at 850 °C	4	120	420	30	0.15	602.5	–	Chen et al. (2021)
Petroleum cokes-based porous carbon	2	1000	60	25	1	159.98	–	Zhu et al. (2018)
Fallen leaves-based porous carbon	2	1000	60	25	1	621.12	–	Zhu et al. (2018)
Chicken feathers-based porous carbon	2	1000	460	25	1	740.74	–	Zhu et al. (2018)
Enteromorpha prolifera-based porous carbon	2	1000	20	25	1	892.86	–	Zhu et al. (2018)

Table 4 (continued)

Adsorbents	pH	C_o (mg L^{-1})	Time (min)	Tem. (°C)	Dose (g L^{-1})	Q_m (mg g^{-1})	RE (%)	References
Porous carbon from $Cu_3(BTC)_2$ pyrolyzed at 700 °C	6	10	240	25	0.5	96.3	100 [a]	Tran et al. (2019a, b, c)
Hierarchical porous carbons from sodium carboxymethyl cellulose	3	150	60	45	0.2	879.68	–	Zhang et al. (2017)
Magnetic hierarchical porous carbon	10	300	250	25	0.2	493.8	–	Dai et al. (2018b)
Magnetic amine-doped hierarchical porous carbon	10	300	250	25	0.2	503.5	–	Dai et al. (2018b)
Magnetic amine-doped hierarchical porous carbon	10	300	250	25	0.2	534.2	–	Dai et al. (2018b)
Shrimp shell-based hierarchical porous carbons	6.94	200	180	45	0.3	742.4	100 [a]	Qin et al. (2016)
Bovine bone-based hierarchical porous carbon	–	150	300	45	0.2	1240	–	Dai et al. (2018a)
Ordered mesoporous carbon–polyethylene glycol	11	400	300	30	1	209.68	–	Mohd Din et al. (2015)
Other adsorbents								
Ionic liquid-modified zeolite	–	1615.66	120	–	50	8.40 [a]	–	Sun et al. (2017)
Ionic liquid-modified illite	–	1615.66	120	–	50	10.34 [a]	–	Sun et al. (2017)
Ionic liquid-modified montmorillonite	–	1615.66	120	–	10	58.16 [a]	–	Sun et al. (2017)
Raw steel shavings	3	1	60	25	2	2.92	100 [a]	Tran et al. (2017)
Nitrogen plasma-modified steel shavings	3	1	60	25	2	3.17	100 [a]	Tran et al. (2017)
Commercial multi-walled carbon nanotubes	3	0.2	720	25	0.06	34.87	–	Zhao et al. (2016)
Commercial aligned multi-walled carbon nanotubes	3	0.2	720	25	0.06	17.1	–	Zhao et al. (2016)
Commercial multi-walled carbon nanotubes	3	0.2	720	25	0.06	8.53	–	Zhao et al. (2016)
Commercial multi-walled carbon nanotubes	3	0.2	720	25	0.06	9.92	–	Zhao et al. (2016)
Commercial multi-walled carbon nanotubes	3	0.2	720	25	0.06	6.59	–	Zhao et al. (2016)

Note that C_o: initial concentration, Tem.: temperature, Q_m: maximum adsorption capacity, RE: removal efficiency, [a] data estimated from the figures of the referred study)

molecules, especially antibiotics (Zhang et al. 2021a, b, c, d). Furthermore, the porosity of porous carbon can be flexibly driven by the activation temperature (Bi et al. 2019). For example, Dai et al. (2018c) manifested that when the activation temperature increased from 750 °C to 900 °C, the surface area and pore volume of mesoporous carbon were improved by 47% and 92%, respectively. In the presence of activators, e.g., alkalis, and strong acids, the porous structure of porous carbons can be enhanced. Indeed, Qin et al. (2016) proved that the mass ratio between KOH and shrimp shell-derived carbon plays a major role in boosting the porosity for hierarchical porous carbons. At high temperature, KOH activator reacts with hydrogen and oxygen-containing groups on the surface of carbons to release the volatile components, e.g., CO_2 and vapor, forming new pores. These results suggested that porous carbon acquires many excellent properties, which may be adequate for the treatment of antibiotic pollution in the aquatic environment.

Metal–organic frameworks

Metal–organic frameworks have received enormous attention from material scientists due to their unique characteristics, e.g., permanent porosity, and extremely high surface area (Deng et al. 2010). As a result, they are widely applied in gaseous fuel storage, chemical hydrogen storage, solar light electrochemical energy storage, and conversion (Li et al. 2020a, b, c, d; Tranchemontagne et al. 2009). The formation mechanism of metal–organic frameworks relies on the coordination between organic ligands and metal ions or clusters (Yaghi et al. 2019). Their homogeneous crystal structure is formed through the linkages of the secondary building units (Safaei et al. 2019). For example, cadmium-based metal–organic frameworks (Cd–TMU–7) were sonochemically synthesized based on binuclear Cd(II) units, $Cd_2(CO_2)_4N_4$, that are six-coordinated and linked through 4,4-oxybisbenzoic acid and 2,5-bis(4-pyridyl)-3,4-diaza-2,4-hexadiene ligands (Masoomi et al. 2017). By possessing inorganic metal ion nodal bonds and organic ligands, metal–organic frameworks can adjust their particle size and shape. Specifically, Vaitsis et al. (2019) observed a remarkable increase up to 23 times in particle size of the magnesium-based metal–organic framework (Mg-MOF-74) synthesized by the solvothermal method in comparison to the ultrasound method.

Considering the outstanding properties of metal–organic frameworks, they can be ideal adsorbents for the removal of chloramphenicol from water. Indeed, Li et al. (2020a, b, c, d) successfully synthesized MIL-53(Al), ZIF-8, UiO-66-NH_2, and NH_2-MIL-125(Ti) by the polydopamine-modified electrospun method. Among these metal–organic frameworks, MIL-53(Al) exhibited the largest surface area, 437.97 $m^2\ g^{-1}$, and pore volume, 0.306 $cm^3\ g^{-1}$, and the best equilibrium chloramphenicol uptake capacity, 79.5 mg g^{-1}. In another study, zirconium-based metal–organic framework (PCN-222) was used as an efficient adsorbent with a very high adsorption capacity of 370 mg g^{-1}, and removal efficiency up to 99% (Zhao et al. 2018). The authors indicated the key role of hydrogen bond and electrostatic interactions as well as the special pore of the adsorbent in elevating the adsorption performance of MIL-53(Al). On the other hand, the desorption efficiency and regeneration of metal–organic frameworks are worth considered since this factor exerts the practical performance of metal–organic framework adsorbents (Abbasi and Rizvandi 2018). The procedure of regeneration is still relatively complex and needs to be meticulously investigated in future researches.

Composites

Composite materials are formed through the process of coordination, functionalization, and cross-linking of precursors to significantly improve the physical, physicochemical, and mechanical properties of the original precursors (Dutt et al. 2020). The composition of composite materials can be divided into two main parts including core and supporting materials that have different properties (Chen et al. 2020a, b). Take carbon-supported nanoscale zero-valent iron composite, for example, the core material is nanoscale zero-valent iron (Li et al. 2021). Although nanoscale zero-valent irons possess a strong ferromagnetic feature, their inherent disadvantage is prone to agglomeration (Lv et al. 2019). To overcome this weakness, the carbon component is added to aid the better dispersion of the nanoscale zero-valent iron particles in the porous carbon matrix (Li et al. 2020a, b, c, d). The strengths of porous carbon are large specific surface area, diversity of functional groups, and high removal performance to pollutants. As a result, the composite in the combination of nanoscale zero-valent iron and porous carbon acquires better physical and physicochemical properties than each single component (Liu and Wang 2019).

According to Table 4, the high efficiency of composite materials for removing chloramphenicol in the aqueous solutions is revealed. For example, Zhang et al. (2013) demonstrated that bovine serum albumin-supported magnetic composite acted as a potential adsorbent for chloramphenicol removal efficiency of 96.4% from water. In another study, Wu et al. (2018) successfully immobilized the nanoscale zero-valent iron particles on activated carbon support, which reached a very high chloramphenicol uptake capacity of 545.25 mg g^{-1}. At the same trend, Xu et al. (2020) found that carbon powder was the best support on nanoscale zero-valent iron. For outcomes of chloramphenicol adsorption, the composite acquired a high removal rate of 3.70 min^{-1}, removal percentage of higher than 99%, and uptake capacity of 3000 mg g^{-1}. It can be therefore concluded that the use of composite materials to treat chloramphenicol from the aquatic environment was considered a promising direction. In further researches, they can extend many emerging applications such as membrane processes, oil–water separation, decomposition of toxic dyes, removal of heavy metals (Ali et al. 2019; Raju and Shanmugaraja 2021).

Molecularly imprinted polymers

Molecularly imprinted polymers are considered emerging materials for solving the problems of competitive adsorption between antibiotics. Their characteristics of adsorption involve high selectivity, magnetic separation, and short time (Fresco-Cala et al. 2020). According to Table 4, polymeric materials exhibited superior adsorption capacities and accelerated equilibrium rates to remove the target pollutants rapidly. To possess outstanding properties, monomers must undergo polymerization under the cross-linking steps to imprint onto the core–shell structure of mesoporous silica

or ferrites through in situ precipitation polymerization (Qin et al. 2020). Researchers demonstrated high performance of molecularly imprinted polymers in the process of removing antibiotics from water. For example, Ma et al. (2020) showed an improvement of chloramphenicol adsorption capacity up to 49.85 mg g^{-1} of porous molecularly imprinted polymers compared with material porous molecularly non-imprinted polymers. Dai et al. (2016) successfully imprinted a homogeneous ultra-thin nanofilm with size of 0.9 nm on the surface of magnetic mesoporous nanosilica to form a novel molecularly imprinted polymer. This adsorbent has a mesoporous structure, microscopic size, high surface area of 542.6 m^2 g^{-1}, and adsorption capacity of 232.6 mg g^{-1} toward acid red dye. Despite their unique properties, the production of molecularly imprinted polymers requires modern machinery, skilled operators, and expensive input materials. As a result, their applications are limited to industrial-scale usage.

Other adsorbents

Apart from the groups of materials mentioned above, Table 4 lists other potential materials to remove chloramphenicol in the aqueous media. First of all, the multi-walled carbon nanotubes are of great interest due to their special structural properties. Kumar et al. (2020) indicated that multi-walled carbon nanotubes were hollow, cylindrically shaped allotropes of carbon, consisting of interlocking single-wall carbon nanotubes. Moreover, the specific surface area and porosity of carbon nanotubes were outstanding, giving enormous benefits for the adsorption of pollutants including pharmaceutical drugs (Carrales-Alvarado et al. 2020). Indeed, Zhao et al. (2016) demonstrated the potential of multi-walled carbon nanotubes for chloramphenicol adsorption. The authors also found that the multi-walled carbon nanotubes having higher surface area of 382 m^2 g^{-1} obtained a better adsorption capacity of 34.87 mg g^{-1}.

Next, some phyllosilicates, e.g., illite, and montmorillonite, and some tectosilicates, e.g., zeolite are worthily considered mineral materials. Sun et al. (2017) successfully modified three materials including illite, montmorillonite, and zeolite using 1–hexadecyl–3-methylimidazolium chloride as a cationic surfactant. After being activated by this ionic liquid, the obtained chloramphenicol adsorption capacity was 58.16 mg g^{-1} for montmorillonite, 10.34 mg g^{-1} for illite, and 8.40 mg g^{-1} for zeolite. The difference among modified adsorbents may be influenced by their cationic exchange capacity, specifically montmorillonite of 1200 mmol kg^{-1}, illite of 140 mmol kg^{-1}, zeolite of 110 mmol kg^{-1}. The higher cationic exchange capacity value the material has, the stronger the adsorption capacity of mineral materials modified by ionic liquids was. The reason was due to the formation of admicelles that support chloramphenicol adsorption.

Finally, the iron-based adsorbents were investigated for their adsorption capacity with chloramphenicol. Ngo et al. (2017) compared the structural change and adsorption results between steel shavings and nitrogen plasma modified steel shavings. The results indicated that the nitrogen plasma method remarkably increased the specific surface area of steel shavings from 2.6916 m^2 g^{-1} to 4.2910 m^2 g^{-1}. There was a slight improvement in the chloramphenicol uptake capacity of nitrogen plasma modified steel shavings of 3.17 mg g^{-1} in comparison with origin raw of 2.92 mg g^{-1}. More importantly, the chloramphenicol removal efficiency of steel shavings modified by nitrogen plasma was reached 100%. It can be commented that the nitrogen plasma method is effective to improve the surface area of the materials, which may directly affect their adsorption performance.

Optimization of chloramphenicol removal

Influential parameters

The chloramphenicol treatment efficiency in water is closely dependent on the properties of each adsorbent as well as the process parameters. The performance of different adsorbents, e.g., porous carbons, metal–organic frameworks, modified polymers, and nanocomposites and experimental conditions for chloramphenicol uptake is summarized in Table 4. There are several influential operating parameters such as initial concentration, adsorbent dosage, system temperature, contact time, and solution pH during the investigation or optimization of chloramphenicol removal. The chloramphenicol treatment efficiency by adsorbents is assessed based on the values of the maximum adsorption capacity and removal efficiency. The maximum chloramphenicol adsorption capacities are obtained from theoretical Langmuir models and experimented values. The chloramphenicol removal efficiency reflects the percentage of chloramphenicol treated by the adsorbents. This section will discuss the effect of operating parameters on the removal of chloramphenicol as illustrated in Fig. 4.

Effect of pH

The pH of the solution is one of the most important factors influencing the adsorption of chloramphenicol in the aqueous solutions. This fact is because pH of the solution is possibly related to the ionization and physicochemical characteristic of chloramphenicol. According to Table 4, the range of pH was investigated mostly from 1 to 12 in the past studies. The protonation of chloramphenicol occurs when pH of the solution is lower than pK_a 5.5 of chloramphenicol (Tian et al. 2017). Specifically, some functional groups, e.g., –OH, –NH–, C=O, and $–NO_2$ of chloramphenicol react with oxygen-containing groups, e.g., –COOH, and C=O of

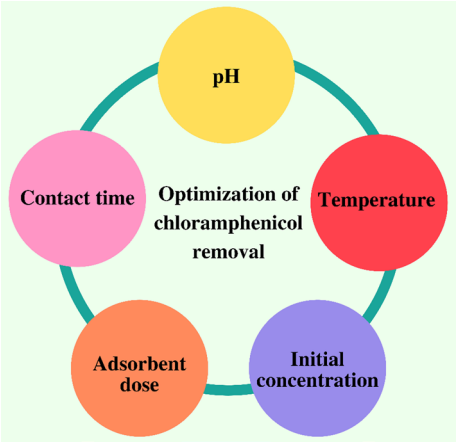

Fig. 4 Effect of operating parameters on the treatment efficient of various adsorbents. In general, solution pH, temperature of adsorption system, initial concentration of chloramphenicol, adsorbent dose, and contact time are considered the most influential operating parameters affecting the removal of chloramphenicol. Here, the optimization of these operating parameters is discussed in detail

the material surface (Zhang et al. 2017). As a result, hydrogen bond is formed between the surface of adsorbent and chloramphenicol, leading to an enhancement in antibiotic adsorption efficiency (Ahmed et al. 2017a, b, c; Li et al. 2018). Indeed, Tran et al. (2019a, b, c) showed that hydrogen bond between metal–organic framework $Fe_3O(BDC)_3$ and chloramphenicol was stronger in acidic solutions, giving the best adsorption efficiency of 11.7 mg L^{-1}. However, increasing the solution pH from 4 to 12 substantially reduced chloramphenicol adsorption. In agreement with Tran et al. (2019a, b, c), Chen et al. (2021) showed that potassium carbonate (K_2CO_3)-modified porous carbon achieved a maximum chloramphenicol adsorption efficiency of 534 mg L^{-1} at pH 4, which was 16% higher than that at pH 9.

On the other hand, the deprotonation of chloramphenicol takes place when the solution has a pH level higher than pK_a 5.5 of chloramphenicol (Qin et al. 2016). During this process, the amide group –NHCO– of chloramphenicol dissociates H^+ or H_3O^+ ions (Xu et al. 2020). The anions dissociated from chloramphenicol exert an attraction force toward the positively charged surface of the adsorbent (Zhao et al. 2018). As a result, the electrostatic interaction is formed, facilitating the adsorption of chloramphenicol in water (Zhang et al. 2017). For example, Tran et al. (2019a, b, c) showed that the mesoporous carbon matrix with pH point of zero charge of 6.4 had a maximum adsorption value of 40.8 mg g^{-1} at the optimum pH 6, which was 46% more efficient than that at pH 3. This result demonstrated that the acidity of the solution is stronger, the electrostatic repulsion between the cationic chloramphenicol and the positively charged adsorbent is prone to reduce the adsorption efficiency. When pH was raised up to 6, the electrostatic repulsion was alleviated, and simultaneously, electrostatic attraction between the negatively charged chloramphenicol and the positively charged mesoporous carbon adsorbent was formed to ameliorate the adsorption of chloramphenicol. In another experiment, Idris et al. (2020) indicated that several materials such as non-imprinted polymers, molecularly imprinted polymers, silica core–shell imprinted polymers, and silica core–shell non-imprinted polymers had strong adsorption capacities at pH between 7 and 8. The adsorption mechanisms by these adsorbents were also proposed based on the electrostatic attraction.

Initial concentration

The initial concentration of chloramphenicol can strongly affect the adsorption capacity of the adsorbents (Chitongo et al. 2019). Generally, the higher the initial concentration of chloramphenicol in solution, the higher the adsorption capacity of adsorbents (Dai et al. 2018c). This fact is consistent with a shift in the concentration gradient, in which chloramphenicol molecules always tend to diffuse from the region having higher concentration—solution to the region having lower concentration—adsorbent until when the system reaches equilibrium (Idris et al. 2020). On the other hand, Zhao et al. (2018) explained that chloramphenicol at higher concentration solution supplied a larger quantity of functional groups, e.g., –OH, $–NO_2$, and C = O, leading to more contact with active sites of $Zr_6(\mu–OH)_8(OH)_8(CO_2)_8$) adsorbent. In this case, hydrogen bond between chloramphenicol and groups, e.g., –OH, and $–COO^-$ of Zr-based metal–organic framework was formed, increasing the adsorption capacity.

The effect of chloramphenicol concentration on adsorption capacity can be monitored by practical experiments. For example, Qin et al. (2016) compared the uptake of chloramphenicol over N-doped hierarchical porous carbons produced from shrimp shells at two different concentrations of 100 and 200 mg L^{-1}. The findings implicated a very high adsorption capacity of 608.1 mg g^{-1} at a concentration of 200 mg L^{-1}, which was 47% higher than that at 100 mg L^{-1}. In another experiment, Tran et al. (2019a, b, c) demonstrated when the initial concentration of chloramphenicol increased from 10 to 40 mg L^{-1}, the adsorption capacity of mesoporous carbons increased. As expected, such mesoporous carbon possessed the highest adsorption capacity of 32.5 mg g^{-1} at the highest concentration of 40 mg L^{-1}.

Contact time

The contact time of chloramphenicol adsorption over the adsorbent is one of the important factors affecting the process kinetic (Ma et al. 2020). Generally, chloramphenicol capture is the strongest at the beginning of the process

and then increases slowly until equilibrium is reached (Wu et al. 2018). This result can be explained by the accelerated diffusion of chloramphenicol filling the micropores of the adsorbent at the first stage. Then, the adsorption sites are gradually occupied until reaching equilibrium nature (Li et al. 2018). As an example, Zhu et al. (2018) described a similar trend of adsorption kinetics among porous carbon materials produced from different precursors, e.g., petroleum cokes, fallen leaves, chicken feathers, and Enteromorpha prolifera. Specifically, the adsorption of chloramphenicol over all adsorbents strongly took place at the first 5-min stage and then steadily increased. However, the equilibrium periods varied among porous carbons, specifically 20 min for Enteromorpha prolifera, 60 min for petroleum cokes and fallen leaves, and 460 min for chicken feather porous carbons. In another experiment, Dai et al. (2018a, b, c) witnessed that porous carbon activated by potassium acetate acquired an adsorption capacity of about 514 mg g^{-1} after 50 min. Meanwhile, there was insignificantly different in adsorption capacity at the equilibrium moment after 250 min since the corresponding value was 556 mg g^{-1}. It is consequently important that optimizing the duration of chloramphenicol adsorption considerably saves time as well as energy.

Temperature

Theoretically, temperature is a measure of the average kinetic energy of the particles, which their kinetic energy and speed increase with increasing temperature (Mohd et al. 2015). Moreover, when the temperature increases, the viscosity of the solutions decreases. This condition enables the molecules to rapidly diffuse through the anti-mass transfer forces and adsorb on the adsorbent (Ma et al. 2020). As a result, temperature is one of the important factors affecting the chloramphenicol adsorption process (Cheng et al. 2019). Many studies demonstrated that increasing temperature contributed to improved adsorption efficiency (Yang et al. 2020a, b; Zhu et al. 2017). For example, Dai et al. (2018a, b, c) investigated the effect of the temperature on the adsorption of chloramphenicol onto the bovine bone-modified porous carbons. As expected, they found that the adsorption capacity obeyed the following order: 1079 mg g^{-1} at 25 °C, 1170 mg g^{-1} at 35 °C, and 1240 mg g^{-1} at 45 °C. In another study, Wu et al. (2018) observed that 50 °C was the optimal temperature for the adsorption of chloramphenicol onto nanoscale zero-valent iron particles supported activate carbon. The results indicated that the maximum adsorption capacity was 1563.97 mg g^{-1} at 50 °C, which was approximately 3 times higher than that at 20 °C.

Adsorbent dose

Considering the effectiveness of an adsorbent, the lower dose, the better. Lower dose of adsorbent brings more advantages such as materials saving and cost-effectiveness. Hence, the optimization of adsorbent dose will be necessary to reduce the material production and treatment costs (Nasseh et al. 2019). Generally, the removal efficiency of chloramphenicol increased with increasing dose of adsorbent (Li et al. 2019). This can be explained by adding a larger amount of adsorbent to the solution, and the adsorption sites are more supplied (Tran et al. 2019a, b, c). This fact increases the chance of contact between chloramphenicol and the absorbent, which also increases the removal efficiency (Chitongo et al. 2019). For example, Lach (2019) investigated the removal efficiency of chloramphenicol by granular activated carbons. The outcomes proved that the maximum removal efficacy of chloramphenicol was 99% at a dose of 8 g L^{-1}, compared with 36% of that at a dose of 1 g L^{-1}. In another experiment, Cheng et al. (2019) pointed out that the chloramphenicol removal efficiency increased from 90 to 100% when the dose of activated carbon produced from corn stover increased from 2 g L^{-1} to 20 g L^{-1}. However, the authors found an optimum dosage at 8 g L^{-1} of corn stover-activated carbon.

Mechanism of chloramphenicol adsorption

The adsorption of chloramphenicol onto the materials is composed of physical and chemical processes (Yang et al. 2020a, b). Therefore, the interaction mechanism between adsorbent and adsorbate is very diverse and dependent on the properties of adsorbent, and experimental conditions. Specifically, surface functional groups, e.g., hydroxyl, carboxyl, and amine on the surface of the adsorbents can cause many interactions with chloramphenicol. Experimental conditions such as solution pH affect the ionization of chloramphenicol. In general, there are several main mechanisms for adsorption of chloramphenicol over carbon adsorbents. Figure 5 illustrates main mechanisms, e.g., electrostatic interaction, hydrogen bonding interaction, Yoshida hydrogen bonding interaction, electron–donor–acceptor interaction, and others for adsorption chloramphenicol over carbon adsorbent as an example. Based on the analysis from Table 4, this section will discuss thoughtfully the mechanisms for the adsorption of chloramphenicol onto adsorbents.

Electrostatic interaction

The electrostatic interaction is a typical mechanism that includes electrostatic attraction and electrostatic repulsion (Idris et al. 2020). The former occurs between positively and negatively charged sites of chloramphenicol and adsorbent

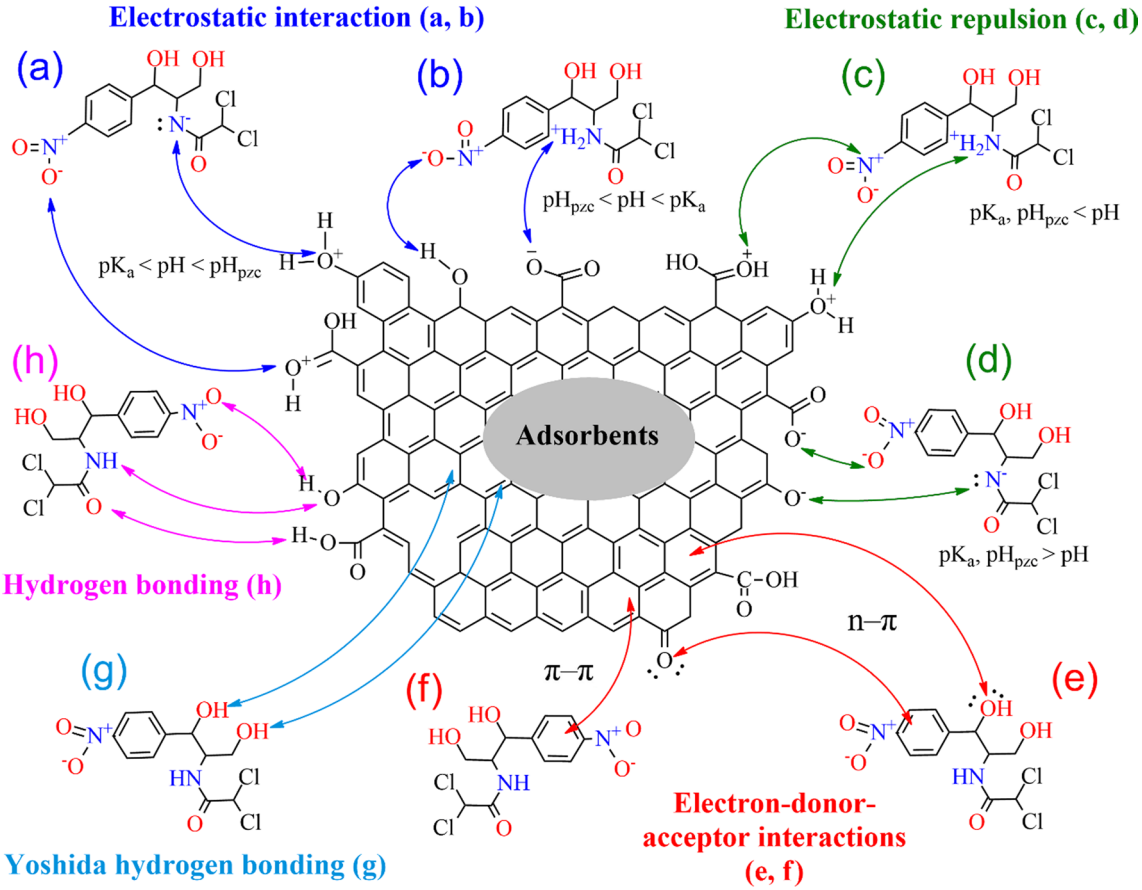

Fig. 5 Possible mechanisms for adsorption of chloramphenicol over carbon adsorbent as an example. Suggested adsorption mechanisms include electrostatic interaction (**a**, **b**), electrostatic repulsion (**c**, **d**), electron–donor–acceptor interaction (**e**, **f**), Yoshida hydrogen bonding interaction (**g**), and hydrogen bonding mechanisms (**h**)

(Yang et al. 2020a, b). Meanwhile, the latter occurs between the same charged sites of chloramphenicol and adsorbent (Ahmed et al. 2017b). As a result, electrostatic attraction enhances the chloramphenicol adsorption and electrostatic repulsion hampers this process (Lach 2019). To elucidate the electrostatic interaction, three key factors including pH point of zero charge of adsorbent pH_{pzc}, solution pH, and pK_a of chloramphenicol should be clarified (Dai et al. 2018c). In detail, pH_{pzc} of adsorbent indicates the surface charge of adsorbent at a certain pH. If the pH is lower than pH_{pzc}, the adsorbent surface will be positively charged and vice versa. If pH is as equal as pH_{pzc}, the adsorbent surface will be neutrally charged at that pH value. pK_a of chloramphenicol can be experimentally determined, as reported at 5.5 (Zhao et al. 2018). When pH is lower than pK_a, chloramphenicol is protonated, becoming a cation. By contrast, when pH is higher than pK_a, chloramphenicol is deprotonated, becoming an anion.

Considering the conditions at pK_a lower than pH and pH lower than pH_{pzc} or pH_{pzc} lower than pH, and pH lower than pK_a, chloramphenicol is deprotonated and negatively charged or anionized, while the surface of adsorbent is positively charged (Fig. 5a, b). As a result, electrostatic attraction occurs to enhance the adsorption of chloramphenicol over the adsorbent. For example, Zhao et al. (2018) found that the pH_{pzc} value of zirconium-based metal–organic framework was 7.0–8.0. At the optimum pH of 6.3, the authors reported the highest removal efficiency was nearly 99%. At the same trend, Tran et al. (2019a, b, c) determined that the pH_{pzc} value of mesoporous carbon produced from metal–organic framework $Fe_3O(BDC)_3$, BDC: benzene-1,4-dicarboxylic acid, was 6.4. The work found that the adsorption of chloramphenicol over this adsorbent gave a maximum adsorption capacity of 96.3 mg g^{-1} at optimum pH 6. These optimum conditions seem to be satisfied with the electrostatic attraction mechanism, and hence, favorable to the adsorption of chloramphenicol.

Considering the conditions at pK_a or pH_{pzc} lower than pH, chloramphenicol is protonated and the surface of adsorbent is positively charged (Fig. 5c). Similarly, under the conditions at pK_a or pH_{pzc} higher than pH, chloramphenicol is deprotonated and the surface of adsorbent is negatively

charged (Fig. 5d). As a result, the electrostatic repulsion intercepts the migration of chloramphenicol on adsorbent, lessening the adsorption efficiency. For example, Tian et al. (2017) reported that the pH_{pzc} value of porous carbons produced from potassium citrate was 4.2. They witnessed a slight decrease in adsorption capacity at pH 3, which may be explained by the repulsion effect between deprotonated chloramphenicol and positively charged carbon adsorbent. Tran et al. (2019a, b, c) found a significantly low chloramphenicol adsorption capacity of 22.2 mg g^{-1} over mesoporous carbon produced from $Fe_3O(BDC)_3$, BDC: benzene-1,4-dicarboxylic acid, at the conditions of pH 3 or pH 8, compared with 40.8 mg g^{-1} at pH 4–6. The same trends were also shown in the previous work (Chen et al. 2021).

Electron–donor–acceptor interactions

Electron–donor–acceptor mechanism is a type of non-covalent interaction that an electron-rich π system can interact with a metal (cationic or neutral), an anion, another molecule, and even another π system (Yi et al. 2020). Considering the uptake of chloramphenicol in the medium, π–π electron–donor–acceptor interactions can be considered as a main adsorption mechanism (Chen et al. 2021). This hypothesis is explained by the chemical structure of chloramphenicol and the functional groups on the surface of the adsorbent (Dai et al. 2018b). Indeed, chloramphenicol possesses a strong electron-withdrawn nitro group $–NO_2$, one amide group –CONH–, two unconjugated alcoholic groups –OH, and an aromatic ring. Meanwhile, several carbon-based adsorbents such as activated carbon, biochar, and porous carbon have many π–electron-rich graphene networks along with functional groups-diverse surface, e.g., –OH, C = O, and –COOH (Ahmed et al. 2017a). In that case, chloramphenicol acts as π–electron–acceptor and the adsorbent acts as π–electron–donor in the adsorption process (Dai et al. 2018c). As a result, an π–π electron–donor–acceptor mechanism between adsorbent and adsorbate can be formed during the adsorption of chloramphenicol (Lach 2019). Moreover, functional groups of adsorbent and chloramphenicol contain lone pairs of electrons on oxygen, or nitrogen, which can lead to a type of n–π electron–donor–acceptor mechanism (Fig. 5e, f). Basically, both types of interactions are less likely to depend on the solution pH.

Many previous works indicated the importance of π–π and n–π electron–donor–acceptor mechanisms in the adsorption of chloramphenicol. For example, Zhu et al. (2018) compared the chloramphenicol adsorption capacity between *Enteromorpha prolifera*-derived and petroleum cokes-derived porous carbons. The results indicated that *Enteromorpha prolifera*-derived porous carbon exhibited an adsorption capacity of 892.86 mg g^{-1}, which was 82% higher than petroleum cokes-derived porous carbon. The authors found that the content of oxygen 12.55% on *Enteromorpha prolifera*-derived porous carbon was so far higher than 6.89% of petroleum cokes-derived porous carbon. This disparity was highly likely to affect the n–π electron–donor–acceptor interaction between porous carbon and chloramphenicol. In another study, Yang et al. (2020a, b) investigated the adsorption of chloramphenicol on peanut shell-based porous biochar. They noted the disappearance of an important peak at 290.9 eV on C 1 s X-ray photoelectron spectroscopy spectrum, corresponding to π–electrons in aromatic rings after chloramphenicol uptake. This finding implied the involvement of π–π electron–donor–acceptor mechanism between aromatic systems in biochar and aromatic ring in chloramphenicol.

Hydrogen bonding

Hydrogen bonding as illustrated in Fig. 5g, h is a type of dipole–dipole attraction between a hydrogen atom covalently bonded to a highly electronegative atom, e.g., N, O, F and another highly electronegative atom (Xiang et al. 2020). Yoshida hydrogen bonding is another interaction between hydrogen atoms covalently bonded to a highly electronegative atom and electrons of aromatic rings (Fig. 5g). According to Table 5, hydrogen bond prevalently exists during the adsorption of chloramphenicol onto the surface of carbon-based materials. Specifically, chloramphenicol in solution contains many functional groups, e.g., –NH, –OH, and $–NO_2$ (Zhao et al. 2016). Meanwhile, the surfaces of adsorbent are filled by oxygen-, nitrogen-containing functional groups, e.g., –OH, –COOH, and –C = O (Qin et al. 2016). As a result, the hydrogen bonding forms an adsorption mechanism, which is effective for chloramphenicol removal (Ahmed et al. 2017a). Apart from dipole–dipole hydrogen bonding, Yoshida hydrogen bonding between adsorbent and chloramphenicol can be also formed. Both dipole–dipole hydrogen bonding and Yoshida hydrogen bonding interactions boost the adsorption of chloramphenicol. For example, Zhao et al. (2018) demonstrated that zirconium-based metal–organic frameworks $Zr_6(\mu\text{-}OH)_8(OH)_8(CO_2)_8$ supplied many –OH groups as adsorption sites. Through dipole–dipole hydrogen bonding and Yoshida hydrogen bonding, these –OH groups interacted with functional groups of each chloramphenicol molecule. As a result, the zirconium-based adsorbent obtained an adsorption capacity of 375 mg g^{-1}, which was so far higher than 10–45 mg/g of other metal–organic frameworks, e.g., MIL-101(Cr), MIL-101(Cr)-NH_2, and MIL-53(Al). To sum up, hydrogen bonds contribute greatly to enhancing the adsorption of chloramphenicol by adsorbent.

However, Li et al. (2018) suggested that hydrogen bonds between chloramphenicol and the surface functional groups of adsorbent could be slightly reduced when the pH values increased. This phenomenon can be explained because

Table 5 Plausible mechanism of chloramphenicol adsorption. Note that data is estimated from the figures of the referred study

Adsorbent	Optimum pH	Adsorption mechanism	References
Sodium hydroxide-modified bamboo charcoal	–	π–π interaction Hydrogen bonding interaction Hydrophobic interaction π–π electron–donor–acceptor interactions	Fan et al. (2010)
Bamboo charcoal-based biochar	7	π–π electron–donor–acceptor interactions Hydrogen bonding interaction Hydrophobic interaction Electrostatic interaction	Liao et al. (2013)
H_3PO_4-activated biochar at 600 °C	4.0–4.5	Electron–donor–acceptor interactions Charge-assisted hydrogen bond Hydrogen bonding interaction Electrostatic interaction	Ahmed et al. (2017b)
H_3PO_4-activated biochar at 600 °C	4.0–4.5	Electron–donor–acceptor interactions Charge-assisted hydrogen bond Hydrogen bonding interaction Electrostatic interaction	Ahmed et al. (2017b)
Peanut shell-based porous biochar	7 [a]	Van der Waals forces π–π interaction Hydrogen bonding interaction Electrostatic interaction	Yang et al. (2020a, b)
H_3PO_4-activated biochar at 600 °C	4.0–4.25	Hydrogen–bonding interaction Electron–donor–acceptor interactions Charge-assisted hydrogen bond	Ahmed et al. (2017a)
Fe_3O_4-functionalized biochar	4.0–4.5	Hydrogen bonding interaction Charge-assisted hydrogen bond Electron–donor–acceptor interactions Electron–acceptor–acceptor interaction	Ahmed et al. (2017a, b, c)
Commercial activated carbon (F–100)	2	Charge-assisted hydrogen bond Electrostatic interaction Electron–donor–acceptor interactions Hydrogen–bonding interaction	Lach (2019)
Commercial activated carbon (WG–12)	2	Charge assisted hydrogen bond Electrostatic interaction Electron–donor–acceptor interactions Hydrogen bonding interaction	Lach (2019)
Commercial activated carbon (ROW 08 Supra)	2	Charge assisted hydrogen bond Electrostatic interaction Electron–donor–acceptor interactions Hydrogen–bonding interaction	Lach (2019)
Commercial activated carbon (Picabiol)	2	Charge-assisted hydrogen bond Electrostatic interaction Electron–donor–acceptor interactions Hydrogen bonding interaction	Lach (2019)
Commercial activated carbon (F–300)	2	Charge-assisted hydrogen bond Electrostatic interaction Electron–donor–acceptor interactions Hydrogen bonding interaction	Lach (2019)
Activated carbon pyrolyzed at 800 °C	2	Charge-assisted hydrogen bond Electrostatic interaction Electron–donor–acceptor interactions Hydrogen bonding interaction	Lach (2019)
Enteromorpha prolifera-based activated carbon	–	π–π electron–donor–acceptor interactions Hydrogen bonding interaction Van der Waals forces	Zhu et al. (2017)

Table 5 (continued)

Adsorbent	Optimum pH	Adsorption mechanism	References
Typha orientalis-based activated carbon	6.2	π–π electron–donor–acceptor interactions Hydrophobic interaction Hydrogen bonding interaction Van der Waals forces Micro-pore filling	Li et al. (2018)
Metal–organic frameworks $Fe_3O(BDC)_3$	4	Metal-bridging interaction Electrostatic attraction π–π interaction Metal-bridging interaction	Van Tran et al. (2019a)
Metal–organic framework PCN–222(Zr)	6.3	Electrostatic interaction Hydrogen bonding interaction	Zhao et al. (2018)
Functional monomer methacrylic acid–molecularly imprinted polymers	8	Electrostatic interaction Hydrophobic interaction Hydrogen bonding Van der Waals interactions	Idris et al. (2020)
Functional monomer methacrylic acid–non-imprinted polymers	8	Electrostatic interaction Hydrophobic interaction Hydrogen bonding Van der Waals interactions	Idris et al. (2020)
Silica core–shell imprinted polymer	8	Electrostatic interaction Hydrophobic interaction Hydrogen bonding Van der Waals interactions	Idris et al. (2020)
Silica core–shell non-imprinted polymers	8	Electrostatic interaction Hydrophobic interaction Hydrogen bonding Van der Waals interactions	Idris et al. (2020)
Core–shell molecularly imprinted polymers based on magnetic chitosan	–	Hydrogen bonding interaction Ionic bonding	Ma et al. (2015)
Core–shell molecularly non-imprinted polymers based on magnetic chitosan	–	Hydrogen bonding interaction Ionic bonding	Ma et al. (2015)
Core–shell surface imprinted nanospheres–magnetic mesoporous nanosilica	–	Hydrogen bonding interaction	Dai et al. (2016)
Potassium citrate-activated porous carbons at 900 °C	9	Van der Waals forces Hydrogen bonding interaction Dipole bond forces Electrostatic interaction Electron–donor–acceptor interactions	Dai et al. (2018c)
Porous carbons from potassium citrate pyrolyzed at 850 °C	11	π–π electron–donor–acceptor interactions Hydrogen bonding interaction Electrostatic interaction Micropore filling	Tian et al. (2017)
Porous carbon pyrolyzed at 800 °C	4	Electrostatic interaction π–π electron–donor–acceptor interactions Hydrogen bonding	Chen et al. (2021)
Petroleum cokes-based porous carbon	2	Electrostatic interaction Electron–donor–acceptor interactions Hydrogen bonding interaction	Zhu et al. (2018)
Fallen leaves-based porous carbon	2	Electrostatic interaction Electron–donor–acceptor interactions Hydrogen bonding interaction	Zhu et al. (2018)
Chicken feathers-based porous carbon	2	Electrostatic interaction Electron–donor–acceptor interactions Hydrogen bonding interaction	Zhu et al. (2018)
Enteromorpha prolifera-based porous carbon	2	Electrostatic interaction Electron–donor–acceptor interactions Hydrogen bonding interaction	Zhu et al. (2018)

Table 5 (continued)

Adsorbent	Optimum pH	Adsorption mechanism	References
Magnetic hierarchical porous carbon	10	π–π electron–donor–acceptor interactions Hydrogen bonding interaction Dipole bonding forces	Dai et al. (2018b)
Hierarchical porous carbons from sodium carboxymethyl cellulose	3	Electron–donor–acceptor interactions Hydrophobic interaction Electrostatic interaction Hydrogen bonding interaction	Zhang et al. (2017)
Shrimp shell-based hierarchical porous carbons	6.94	Van der Waals forces Hydrogen bonding interaction π– π electron–donor–acceptor interactions	Qin et al. (2016)
Porous carbon from $Cu_3(BTC)_2$ pyrolyzed at 700 °C	6	Hydrogen bonding interaction Electrostatic attraction π–π interaction Metal-bridging interaction	Tran et al. (2019a, b, c)
Nanosized zero-valent iron functionalized biochar	4.0–4.5	Charge-assisted hydrogen bond Hydrogen bonding interaction Electron–donor–acceptor interactions	Ahmed et al. (2017a, b, c)
Activated carbon-supported nanoscale zero-valent iron	7	Electrostatic interactions	Xu et al. (2020)
Multi-walled carbon nanotubes-supported nanoscale zero-valent iron	7	Electrostatic interactions	Xu et al. (2020)
Carbon powder-supported nanoscale zero-valent iron	7	Electrostatic interactions	Xu et al. (2020)
Biochar supported nanoscale zero-valent iron	7	Electrostatic interactions	Xu et al. (2020)
Graphene oxide supported nanoscale zero-valent iron	7	Electrostatic interactions	Xu et al. (2020)
Ordered mesoporous carbon–polyethylene glycol	11	Electron–donor–acceptor interactions Hydrogen bonding interaction	Mohd et al. (2015)
Commercial multi-walled carbon nanotubes	3	Electron–donor–acceptor interactions Hydrogen bonding interaction The Lewis acid–base interaction	Zhao et al. (2016)
Commercial multi-walled carbon nanotubes	3	Electron–donor–acceptor interactions Hydrogen bonding interaction The Lewis acid–base interaction	Zhao et al. (2016)
Commercial multi-walled carbon nanotubes	3	Electron–donor–acceptor interactions Hydrogen bonding interaction The Lewis acid–base interaction	Zhao et al. (2016)
Commercial multi-walled carbon nanotubes	3	Electron–donor–acceptor interactions Hydrogen bonding interaction The Lewis acid–base interaction	Zhao et al. (2016)
Commercial multi-walled carbon nanotubes	3	Electron–donor–acceptor interactions Hydrogen bonding interaction The Lewis acid–base interaction	Zhao et al. (2016)
Raw steel shavings	3	Hydrogen bonding interaction Electrostatic interactions Non-electrostatic interactions	Tran et al. (2017)
Nitrogen plasma-modified steel shavings	3	Hydrogen bonding interaction Electrostatic interactions Non-electrostatic interactions	Tran et al. (2017)

acidic functional groups, e.g., –COOH, of carbon-based adsorbents are gradually ionized ($–COO^-$) at higher pH. Hence, H_2O molecules competed with charged functional groups of chloramphenicol molecules. Agreed with the above hypothesis, Lach (2019) found that the adsorption capacity of chloramphenicol onto granular activated carbons had a slight decrease from 200 mg/g to 180 mg/g with increasing pH from 2 to 10. The reduced quantity of surface functional groups on granular activated carbon at higher pH conditions might lower the attractive force of hydrogen bonding, thereby, unconducive to adsorption.

Other mechanisms

Hydrophobic mechanism is a type of interaction between nonpolar molecules together. They usually have a long chain

of aliphatic carbons or aromatic rings that do not interact with water molecules (Geng et al. 2021). Therefore, taking advantage of high hydrophobicity of chloramphenicol to remove it from water by hydrophobic adsorbents such as activated carbons and biochars by adsorption methods should not be ignored (Zhang et al. 2017). Accordingly, Idris et al. (2020) suggested that high binding capacities of chloramphenicol by imprinted polymers were attributable mainly to strong hydrophobic interactions. Hydrophobic effect of imprinted polymers on chloramphenicol adsorption significantly boosted, leading to an increase in the non-specific template binding. Through the desorption process, Li et al. (2018) demonstrated the presence of hydrophobic interaction in the adsorption of chloramphenicol onto *Typha orientalis* activated carbon. Indeed, they used 95% ethanol to perform the recovery of chloramphenicol from the adsorbent material. As expected, approximately 40% of chloramphenicol was desorbed, whereas desorption with distilled water was only 11%.

Along with chemical adsorption, physical adsorption also contributes significantly to the enhanced removal of chloramphenicol by adsorbent materials (Yang et al. 2020a, b). Physical adsorption is a type of mechanism that depends majorly on the structure of the adsorbent, e.g., surface area, and pores (Zhu et al. 2017). Based on Table 5, physical adsorption mechanisms such as van der Waals forces, and micropore-filling markedly control chloramphenicol absorption. Micropore filling is the process by which chloramphenicol molecules are adsorbed into micropores of the adsorbent (Yang et al. 2020a, b). For instance, Tian et al. (2017) estimated the size of chloramphenicol molecule at 0.436 nm. Whereas the average pore diameter of potassium citrate-activated porous carbons was measured at 1.921 nm, and adequate for chloramphenicol adsorption. As expected, the kinetic adsorption of potassium citrate-activated porous carbons for chloramphenicol was about 475 mg g^{-1}. In another experiment, Li et al. (2018) observed a notable decrease in micropore volume of activated carbon from 0.154 to 0.106 cm^3 g^{-1} after chloramphenicol adsorption. It can be therefore concluded that chloramphenicol molecules tend to fill the pores of the adsorbent.

The van der Waals forces between chloramphenicol and adsorbent are basically weak and reversible interactions (Yang et al. 2020a, b). In accordance with this argument, Dai et al. (2018a, b, c) demonstrated van der Waals forces as a weak binding force through competitive adsorption between chloramphenicol and humic acid on the surface of the adsorbent. The results indicated that the adsorption capacity of chloramphenicol over potassium acetate-activated porous carbons in the absence of humic acid was 548.21 mg g^{-1}. In the presence of humic acid, the adsorption efficiency was 215.04 mg g^{-1}, suggesting a remarkable decrease of 61%. This phenomenon can be explained by breaking the van der Waals forces bonds between chloramphenicol and porous carbons. In another study, Qin et al. (2016) suggested that the formation of van der Waals forces between shrimp shell-based porous carbons and chloramphenicol could influence the adsorption capacity. They noticed that porous carbons with a tremendous specific surface area of 3171 m^2 g^{-1}, and a large pore volume of 1.934 cm^3 g^{-1} enhanced the adsorbent interfaces, improving van der Waals forces, hence better contacting with chloramphenicol. As expected, porous carbons reached a maximum kinetic adsorption capacity of 475 mg g^{-1}.

Equilibrium isotherm, kinetic, thermodynamic models

Isotherm models

In general, the adsorption isotherm models are used to describe the relationship between adsorbate concentration and adsorption capacity at the equilibrium. They can supply some assumptions of adsorption mechanism of the adsorbate on the surface of the adsorbent when the process reaches equilibrium (Zhang et al. 2017). After solving isotherm models, the estimation of maximum adsorption capacity can be determined. This indicator assesses the performance of the adsorbents, and some properties of porous solid adsorbents (Dai et al. 2016). The adsorption isotherm models can be described in the linear or nonlinear form of mathematical regression equations (Cheng et al. 2019; Idris et al. 2020). For linear isotherms, the coefficient of determination R^2 is the most important parameter to select the best-fitted model. Meanwhile, nonlinear isotherms are characteristic of multiple iterative procedures, which were employed by computer software to obtain the most reliable estimation (Lach 2019; Tran et al. 2017). Apart from R^2 value, several common error functions, e.g., hybrid fractional error function, squares of the errors, mean relative error, and Marquardt's percent standard deviation can be used to assess the reliability and compatibility of each nonlinear model (Fig. 6). Generally, the lower error function values and higher R^2 value, the better fitted models. It is also found from Table 6 that linear isotherms are more frequently used than nonlinear models. This fact may be the simplicity and flexibility of fitting linear regressions than nonlinear ones.

There are several common isotherm models involving Langmuir, Freundlich, Temkin, Dubinin–Radushkevich, Redlich–Peterson, and Sips (Fig. 7). Table 6 shows that Langmuir and Freundlich isotherms emerged mostly as the best fit models for describing chloramphenicol uptake by the various adsorbents. This observation underscores the fact that materials with homogeneous monolayer or heterogeneous multi-layer surfaces have a predominance of chloramphenicol adsorption. It is also witnessed that R^2 values are

Error functions	Mathematical description	
Coefficient of determination	$R^2 = \frac{\sum_{i=1}^{n}(Q_{i,\exp} - \overline{Q_{i,\exp}})^2 - \sum_{i=1}^{n}(Q_{i,\exp} - \overline{Q_{i,cal}})^2}{\sum_{i=1}^{n}(Q_{i,\exp} - \overline{Q_{i,\exp}})^2}$	1
Mean relative error	$MRE\,(\%) = \frac{100}{n}\sum_{i=1}^{n}\left\lvert\frac{Q_{i,cal} - Q_{i,\exp}}{Q_{i,\exp}}\right\rvert$	2
Squares of the errors	$SSE = \sum_{i=1}^{n}\left(Q_{i,cal} - Q_{i,\exp}\right)^2$	3
Hybrid fractional error function	$HYBRID = \frac{100}{n-p}\sum_{i=1}^{n}\left\lvert\frac{\left(Q_{i,cal} - Q_{i,\exp}\right)^2}{Q_{i,\exp}}\right\rvert$	4
Marquardt's percent standard deviation	$MPSD = 100\sqrt{\frac{1}{n-p}\sum_{i=1}^{n}\left(\frac{Q_{i,cal} - Q_{i,\exp}}{Q_{i,\exp}}\right)^2}$	5

Fig. 6 Mathematic form of common error functions including coefficient of determination, R^2; mean relative error, MRE; squares of the errors, SSE; hybrid fractional error function, HYBRID; and Marquardt's percent standard deviation, MPSD. Chloramphenicol adsorption capacity values are called as $Q_{i,cal}$ and $Q_{i,exp}$ corresponding to calculated and experimental values, respectively; mean theoretical and experimental adsorption capacity values are called $\overline{Q_{i,exp}}$ and $\overline{Q_{i,cal}}$, respectively; n is the total number of experimental data points, and n_p is the total number of parameters of each kinetic or isotherm model

very high, between 0.9 and 1.0. A considerable number of works adopt linear isotherms regardless of possible inaccuracy of estimation. Conversely, some researchers solved the nonlinear isotherms and assessed their validation using function errors (Tran et al. 2019b; Yang et al. 2020a, b). This will increase the accuracy and reliability of estimations. The results of maximum chloramphenicol adsorption capacity are mainly calculated by Langmuir isotherm.

Kinetic models

Adsorption kinetics supply information about the uptake of chloramphenicol onto the adsorbent with respect to contact time. The models of kinetics can be categorized by reaction and diffusion types. The former type describes chemically kinetic reactions over time without including steps. Meanwhile, the latter is characteristic of main stages such as (i) film diffusion: the process that chloramphenicol occurs across the surrounding of adsorbent; (ii) intraparticle diffusion: the migration of chloramphenicol on the surface of adsorbent; (iii) the adsorption and desorption of chloramphenicol with active sites of the adsorbent. Kinetic models reflect the rate of chloramphenicol adsorption and desorption processes, which are modelized by mathematical equations. Similar to adsorption isotherms, linear and nonlinear mathematical forms of kinetic models have been developed. Various mathematical forms of linear and nonlinear models involving pseudo-first-order, pseudo-second-order, Elovich, and Bangham can be referred from Fig. 8.

According to Table 6, previous works claim the compatibility of chloramphenicol adsorption kinetics models in both linear and nonlinear mathematical forms with high R^2 values. The predominance of linear isotherms rather than nonlinear models can be due to their simplicity and flexibility of fitting linear regressions than nonlinear ones. Moreover, chloramphenicol adsorbed onto different material surfaces majorly fits best with the pseudo-second-order model among the other ones, e.g., pseudo-first-order, Elovich, and Bangham. The pseudo-second-order model assumes that chemisorption is controlled by functional groups of chloramphenicol and adsorbent through rate-limiting steps. However, there is still debate on what form of pseudo-second-order equations should be applied to avoid possible errors. Many studies pointed out that the linear form of this equation was the most suitable for the adsorption kinetic of chloramphenicol (Ma et al. 2015; Wu et al. 2018). In contrast, (Li et al. 2020a, b, c, d) proved that nonlinear pseudo-second-order equations were successful in describing solid–liquid chloramphenicol adsorption system. Lima et al. (2021) recommended that future investigations should adopt computer software to fit nonlinear equations for better accurate results.

Thermodynamic models

In this section, the influence of temperature on chloramphenicol adsorption and the property of thermodynamic process are elucidated. Referring to thermodynamic parameters, the spontaneity and heat of chloramphenicol adsorption over the adsorbent can be better understood (Chen et al. 2021; Dai et al. 2018a). Characteristic parameters affecting the process involve Gibbs free energy ΔG°, enthalpy ΔH°, and entropy ΔS° (Yang et al. 2020a, b; Zhang et al. 2021a, b, c, d). Mathematically, they are originated from classical Van 't Hoff expression, represented by the following equations (Eqs. 26–28).

$$\ln K_{eq} = \frac{\Delta S^{\circ}}{R} - \frac{\Delta H^{\circ}}{RT} \tag{26}$$

$$\Delta G^{\circ} = -RT\ln K_{eq} \tag{27}$$

$$\Delta G^{\circ} = (\Delta H^{\circ} - T\Delta S^{\circ}) \tag{28}$$

where K_{eq} is equilibrium kinetic rate constant; T is the temperature in Kelvin; R is the universal gas constant,

Table 6 Isotherm and kinetic models for chloramphenicol adsorption. Note that R^2: coefficient of determination, PSO: pseudo-second-order

Adsorbent	Isotherm models			Kinetic models			References
	Adherence	Type	R^2	Adherence	Type	R^2	
Porous carbon from $Cu_3(BTC)_2$ pyrolyzed at 700 °C	Freundlich	Nonlinear	0.993	PSO	Linear	0.991	Tran et al. (2019a, b, c)
Potassium citrate–activated porous carbons at 900 °C	Langmuir	Linear	1.000	PSO	Linear	1.000	Dai et al. (2018c)
Porous carbons from potassium citrate pyrolyzed at 750 °C	Langmuir	Linear	0.991	PSO	Linear	0.992	Tian et al. (2017)
Porous carbons from potassium citrate pyrolyzed at 800 °C	Langmuir	Linear	0.993	PSO	Linear	0.995	Tian et al. (2017)
Porous carbons from potassium citrate pyrolyzed at 850 °C	Langmuir	Linear	0.995	PSO	Linear	0.993	Tian et al. (2017)
Porous carbons from potassium citrate pyrolyzed at 900 °C	Langmuir	Linear	0.990	PSO	Linear	0.991	Tian et al. (2017)
Petroleum cokes-based porous carbon	Langmuir	Linear	0.991	PSO	Linear	0.998	Zhu et al. 2018)
Fallen leaves-based porous carbon	Langmuir	Linear	0.998	PSO	Linear	1.000	(Zhu et al. 2018)
Chicken feathers-based porous carbon	Langmuir	Linear	0.999	PSO	Linear	0.999	Zhu et al. (2018)
Enteromorpha prolifera-based porous carbon	Langmuir	Linear	0.999	PSO	Linear	1.000	Zhu et al. (2018)
Hierarchical porous carbons from sodium carboxymethyl cellulose	Langmuir	Linear	0.999	PSO	Linear	0.999	Zhang et al. (2017)
Bovine bone-based hierarchical porous carbon	Langmuir	Nonlinear	0.999	PSO	Linear	1.000	Dai et al. (2018a)
Shrimp shell-based hierarchical porous carbons	Langmuir	Linear	1.000	PSO	Linear	1.000	Qin et al. (2016)
Magnetic amine-doped hierarchical porous carbon	Langmuir	Linear	0.997	PSO	Linear	0.993	Dai et al. (2018b)
Magnetic amine-doped hierarchical porous carbon	Langmuir	Linear	0.998	PSO	Linear	0.997	Dai et al. (2018b)
Magnetic amine-doped hierarchical porous carbon	Langmuir	Linear	0.999	PSO	Linear	0.995	Dai et al. (2018b)
KOH-activated carbon	Langmuir	Linear	0.996	PSO	Linear	0.998	Wu et al. (2018)
Commercial activated carbon (F–300)	Langmuir	Linear	0.996	PSO	Linear	0.989	Lach and Kubicka (2017)
Commercial activated carbon (F–300)	Langmuir	Nonlinear	0.993	PSO	Nonlinear	0.975	Lach (2019)
Commercial activated carbon (F–100)	Langmuir	Nonlinear	0.968	PSO	Nonlinear	0.954	Lach (2019)
Commercial activated carbon (WG–12)	Langmuir	Nonlinear	0.987	PSO	Nonlinear	0.968	Lach (2019)
Commercial activated carbon (ROW 08 Supra)	Langmuir	Nonlinear	0.995	PSO	Nonlinear	0.988	Lach (2019)
Commercial activated carbon (Picabiol)	Langmuir	Nonlinear	0.996	PSO	Nonlinear	0.994	Lach (2019)
Hydrochloric acid-activated grape slurry waste	Langmuir	Linear	0.959	PSO	Linear	0.817	Chitongo et al. (2019)
KOH-activated grape slurry waste	Langmuir	Linear	0.978	PSO	Linear	0.982	Chitongo et al. (2019)
Enteromorpha prolifera-based activated carbon	Langmuir	Linear	0.999	–	–	–	Zhu et al. (2017)
Typha orientalis-based activated carbon	Freundlich	Nonlinear	0.998	PSO	Linear	1.000	Li et al. (2018)
Corn stover-based activated carbon	Langmuir	Nonlinear	0.999	PSO	Linear	1.000	Cheng et al. (2019)
Porous carbon pyrolyzed at 800 °C	Langmuir	Nonlinear	0.998	PSO	Nonlinear	0.993	Chen et al. (2021)
Commercial powdered activated carbon	Langmuir	Linear	0.987	PSO	Linear	0.999	Zhang et al. (2021a, b, c, d)
Bamboo charcoal-based biochar	Freundlich	Nonlinear	0.975	–	–	–	Liao et al. (2013)
Bamboo charcoal-based biochar	Langmuir	Nonlinear	0.970	–	–	–	Ahmed et al. (2017b)
Biochars pyrolyzed at 350 °C	Langmuir	Nonlinear	0.998	PSO	Linear	1.000	Yang et al. (2020a, b)
Biochars pyrolyzed at 500 °C	Langmuir	Nonlinear	0.954	PSO	Linear	0.962	Yang et al. (2020a, b)
Biochars pyrolyzed at 700 °C	Langmuir	Nonlinear	0.888	PSO	Linear	0.982	Yang et al. (2020a, b)
Peanut shell-based porous biochar	Langmuir	Nonlinear	1.000	PSO	Linear	0.999	Yang et al. (2020a, b)

Table 6 (continued)

Adsorbent	Isotherm models			Kinetic models			References
H_3PO_4-activated functionalized biochar at 600 °C	Langmuir	Nonlinear	0.990	–	–	–	Ahmed et al. (2017b)
H_3PO_4-activated biochar at 600 °C	Langmuir	Nonlinear	0.98	–	–	–	Ahmed et al. (2017b)
H_3PO_4-activated biochar at 600 °C	Freundlich	Nonlinear	0.925	PSO	Nonlinear	0.991	Ahmed et al. (2017a)
Nanosized zero-valent iron functionalized biochar	Langmuir	Nonlinear	0.991	–	–	–	Ahmed et al. (2017a, b, c)
Ionic liquid-modified zeolite	–	–	–	PSO	Nonlinear	1.000	Sun et al. (2017)
Ionic liquid-modified illite	–	–	–	PSO	Nonlinear	1.000	Sun et al. (2017)
Ionic liquid-modified montmorillonite	–	–	–	PSO	Nonlinear	1.0000	Sun et al. (2017)
Functional monomer methacrylic acid–molecularly imprinted polymers	Freundlich	Linear	1.000	PSO	Linear	1.000	Idris et al. (2020)
Functional monomer methacrylic acid–non- imprinted polymers	Freundlich	Linear	0.993	PSO	Linear	1.000	Idris et al. (2020)
Silica core–shell imprinted polymer	Langmuir	Linear	0.999	PSO	Linear	1.000	Idris et al. (2020)
Silica core–shell non-imprinted polymer	Langmuir	Linear	0.987	PSO	Linear	0.988	Idris et al. (2020)
Porous molecularly imprinted polymer using halloysite nanotube	Freundlich	Linear	0.997	PSO	Linear	1.000	Ma et al. (2020)
Porous molecularly non-imprinted polymer using halloysite nanotube	Freundlich	Linear	0.996	PSO	Linear	0.999	Ma et al. (2020)
Core–shell molecularly imprinted polymers based on magnetic chitosan	Langmuir	Nonlinear	0.999	PSO	Linear	0.998	Ma et al. (2015)
Core–shell molecularly non-imprinted polymers based on magnetic chitosan	Langmuir	Nonlinear	0.998	PSO	Linear	0.997	Ma et al. (2015)
Core–shell surface imprinted nanospheres–magnetic mesoporous nanosilica	Freundlich	Linear	0.996	PSO	Linear	1.000	Dai et al. (2016)
Core–shell surface non-imprinted nanospheres–magnetic mesoporous nanosilica	Freundlich	Linear	0.999	PSO	Linear	1.000	Dai et al. (2016)
Metal–organic framework $Fe_3O(BDC)_3$	Langmuir	Nonlinear	0.993	PSO	Linear	0.993	Tran et al. (2019a, b, c)
Metal–organic framework–PCN–222(Zr)	–	–	–	PSO	Linear	0.999	Zhao et al. (2018)
Porous carbon from $Cu_3(BTC)_2$ pyrolyzed at 700 °C	Langmuir	Nonlinear	0.997	PSO	Linear	0.998	Tran et al. (2019a, b, c)
Raw steel shavings	Langmuir	Linear	0.981	PSO	Linear	0.972	Tran et al. (2017)
Plasma-modified steel shavings	Langmuir	Linear	0.923	PSO	Linear	0.974	Tran et al. (2017)
Ordered mesoporous carbon–polyethylene glycol	Langmuir	Nonlinear	0.905	PSO	Nonlinear	0.999	Mohd Din et al. (2015)
Metal–organic framework MIL–53(Al)	Langmuir	Nonlinear	0.994	PSO	Nonlinear	0.990	Li et al. (2020a, b, c, d)
Metal–organic framework ZIF–8	Langmuir	Nonlinear	0.978	PSO	Nonlinear	0.958	Li et al. (2020a, b, c, d)
Metal–organic framework UiO–66-NH_2	Langmuir	Nonlinear	0.989	PSO	Nonlinear	0.944	Li et al. (2020a, b, c, d)
Metal–organic framework NH_2–MIL–125(Ti)	Langmuir	Nonlinear	0.994	PSO	Nonlinear	0.877	Li et al. (2020a, b, c, d)
Fe_3O_4-functionalized biochar	Langmuir	Nonlinear	0.968	–	–	–	Ahmed et al. (2017a, b, c)
Commercial multi–walled carbon nanotubes	Freundlich	Nonlinear	0.994	PSO	Linear	1.000	Zhao et al. (2016)
Commercial multi–walled carbon nanotubes (Aligned–MWCNT)	Freundlich	Nonlinear	0.994	PSO	Linear	1.000	Zhao et al. (2016)
Commercial multi-walled carbon nanotubes (S–MWCNT–2040)	Freundlich	Nonlinear	0.982	PSO	Linear	1.000	Zhao et al. (2016)
Commercial multi-walled carbon nanotubes (L–MWCNT–2040)	Freundlich	Nonlinear	0.985	PSO	Linear	1.000	Zhao et al. (2016)

Table 6 (continued)

Adsorbent	Isotherm models			Kinetic models			References
Commercial multi-walled carbon nanotubes (L–MWCNT–60100)	Freundlich	Nonlinear	0.985	PSO	Linear	1.000	Zhao et al. (2016)
Fe_3O_4-supported bovine serum albumin	Langmuir	Linear	0.989	PSO	–	–	Zhang et al. (2013)
Nanoscale zero-valent iron particles supported activated carbon	Langmuir	Linear	0.998	PSO	Linear	0.996	Wu et al. (2018)
Activated carbon-supported nanoscale zero-valent iron	Langmuir	Nonlinear	0.986	PSO	Linear	1.000	Xu et al. (2020)
Multi-walled carbon nanotubes-supported nanoscale zero-valent iron	Langmuir	Nonlinear	0.922	PSO	Linear	0.999	Xu et al. (2020)
Carbon powder-supported nanoscale zero-valent iron	Langmuir	Nonlinear	0.999	PSO	Linear	0.999	Xu et al. (2020)

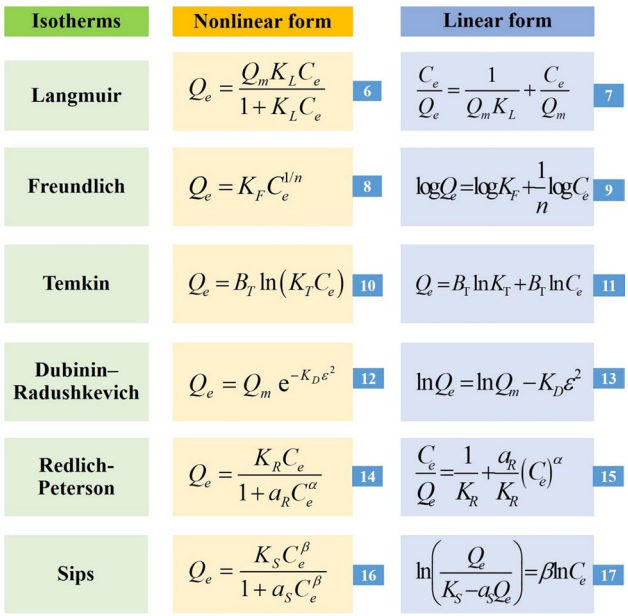

Fig. 7 Common isotherm models involving Langmuir, Freundlich, Temkin, Dubinin–Radushkevich, Redlich–Peterson, and Sips. Parameters of each isotherm model are defined as follows; Q_e (mg g^{-1}) and Q_m (mg g^{-1}) are the equilibrium and maximum adsorption capacity values; C_e (mg L^{-1}) is the post-adsorption concentration of chloramphenicol remaining at the equilibrium moment; K_L (L mg^{-1}) is the constant coefficient Langmuir; $R_L = \frac{1}{1+C_o K_L}$ is the separation factor, C_o is the initial concentration; the process is unfavorable if r_L is higher than 1, linear if r_L is equal to 1, favorable if r_L lower than 1, and irreversible if r_L is zero; K_F [(mg g^{-1}) (L $mg^{-1})^n$] is the Freundlich constant; 1/n is the adsorption intensity constant that reveals either one-layer adsorption if n is lower than 1 or multi-layer adsorption if n is higher than 1; k_T (L g^{-1}) is the Temkin isotherm constant; B_T (mg g^{-1}) is related to adsorption heat; K_D (L mg^{-1}) is the Dubinin–Radushkevich isotherm constant;ε (kJ mol^{-1}) is the Polanyi potential in the Dubinin–Radushkevich equation; K_R (L mg^{-1}) and a_R (L g^{-1}) are the Redlich–Peterson isotherm constants; α is the Redlich–Peterson isotherm exponent; K_S (L mg^{-1}) and a_S (L g^{-1}) are the Sips isotherm constants; β is the Sips isotherm exponent

of 8.314 J mol^{-1} K^{-1}; K_{eq} is calculated from the experimental results of adsorption isotherms at different temperatures; ΔG°, ΔH°, and ΔS° are Gibbs free energy (kJ mol^{-1}), standard enthalpy (kJ mol^{-1}), and standard entropy (kJ mol^{-1} K^{-1}), respectively; if ΔG° is lower than 0, chloramphenicol uptake is thermodynamically spontaneous, and vice versa if ΔG° is higher than 0, it is thermodynamically nonspontaneous; if ΔH° is higher than 0, the adsorption is endothermic, and vice versa, ΔH° is lower than 0, the adsorption is exothermic; if ΔS° is higher than 0, there is an increasing trend in disorderliness leading to better chloramphenicol uptake rate, and vice versa if ΔS° is lower than 0, it reflects a decreasing trend in the disorderliness of chloramphenicol uptake.

Table 7 briefly presents the thermodynamic parameters of chloramphenicol uptake by various adsorbents. In general, the temperature for investigation of the adsorption process is varied in the range from 288 to 323 K. This range of temperature is favorable for treatment activities under large-scale adsorption conditions. In addition, the magnitudes of thermodynamic parameters provide information on the nature of chloramphenicol adsorption. According to Table 7, the chloramphenicol adsorption over most absorbents is a thermodynamically spontaneous and endothermic process since ΔG° is between − 9.01 and − 0.03 kJ mol^{-1}, and ΔH° is between 0.031 and 49.0 kJ mol^{-1}. Most chloramphenicol uptakes are also the processes that increase in disorderliness since ΔS° is between 0.028 and 5.212 kJ mol^{-1} K^{-1}. By contrast, some works revealed a different trend in thermodynamic data. For example, the exothermic nature of the chloramphenicol uptake over both metal–organic framework $Fe_3O(BDC)_3$ and mesoporous carbon was described because ΔH° was lower than zero (Tran et al. 2019a). Considering the thermodynamic data of the chloramphenicol adsorption over powdered activated carbon, Zhang et al., (2021a, b,

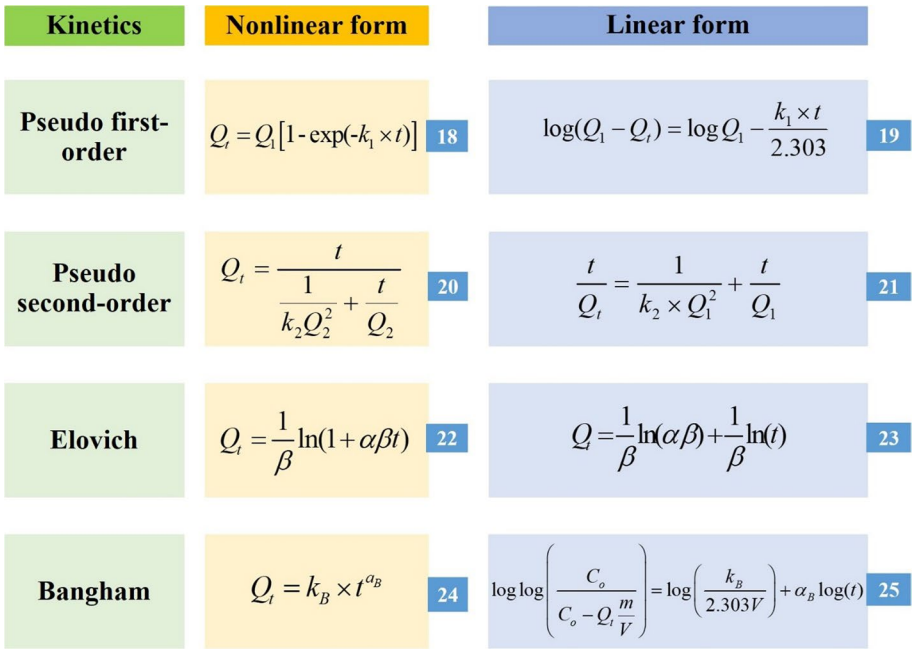

Fig. 8 Common linear and nonlinear kinetic models including pseudo-first-order, pseudo-second-order Elovich, and Bangham. Parameters of each isotherm model are defined as follows; t (min) is the time of adsorption process; m (g) and V (L) are the weight of adsorbent and volume of solution, respectively; Q_1 (mg g^{-1}) and Q_2 (mg g^{-1}) are the adsorption capacity values of pseudo-first-order kinetic, and pseudo-second-order kinetic at the equilibrium moment, respectively; Q_t (mg g^{-1}) is the adsorption capacity value at the time t; α (mg g^{-1} min^{-1}) and β (g mg^{-1}) are the adsorption rate and desorption rate constants, respectively; k_1 (min^{-1}) and k_2 (g mg^{-1} min^{-1}) are the pseudo-first-order and pseudo-second-order rate constants, respectively; k_B and α_B are Bangham constants

Table 7 Thermodynamic modeling for chloramphenicol adsorption. Note that Tem.: temperature, ΔG°: standard Gibbs free energy, ΔH°: standard enthalpy, ΔS°: standard entropy

Adsorbent	Thermodynamic parameters				References
	Temp (K)	ΔG° (kJ/mol)	ΔH° (kJ/mol)	ΔS° (kJ/mol K^{-1})	
Potassium citrate-activated porous carbons at 900 °C	288	−5.774	9.087	0.052	Dai et al. (2018c)
Porous carbons from potassium citrate pyrolyzed at 850 °C	288	−3.611	32.48	0.125	Tian et al. (2017)
Porous carbon pyrolyzed at 800 °C	298	−6.2419	13.79	0.067	Chen et al. (2021)
Hierarchical porous carbons from sodium carboxymethyl cellulose	308	−6.335	7.121	0.044	Zhang et al. (2017)
Magnetic amine-doped hierarchical porous carbon	298	−5.649	2.776	0.028	Dai et al. (2018b)
Bovine bone-based hierarchical porous carbon	308	−6.748	0.02516	1.001	Dai et al. (2018a)
Shrimp shell-based hierarchical porous carbons	298	–6.447	0.0379	4.86	Qin et al. (2016)
KOH-activated carbon	323	−5.298	17.558	0.07	Wu et al. (2018)
Commercial powdered activated carbon	298	2.031	28.74	0.0898	Zhang et al. (2021a, b, c, d)
Peanut shell–based porous biochar	303	−2.519	0.03137	5.212	Yang et al. (2020a, b)
Metal–organic framework $Fe_3O(BDC)_3$	298	−2.8933	−13.895	−0.0369	Tran et al. (2019a, b, c)
Porous carbon from $Cu_3(BTC)_2$ pyrolyzed at 700 °C	298	−0.03	−25.443	−0.0685	Tran et al. (2019a, b, c)
Raw steel shavings	293	−5.319	−7.494	−0.007	Tran et al. (2017)
Plasma-modified steel shavings	293	−5.326	−0.667	0.016	Tran et al. (2017)
Ordered mesoporous carbon–polyethylene glycol	303	−9.01	49	0.12	Mohd et al. (2015)
Nanoscale zero-valent iron particles supported activated carbon	323	−4.803	11.232	0.05	Wu et al. (2018)

c, d) found a thermodynamically nonspontaneous process because ΔG° was higher than zero. Moreover, negative values of ΔS° were overwhelmingly dominant in some chloramphenicol adsorption systems using metal–organic framework and raw steel shavings (Tran et al. 2017, 2019a).

Desorption and regeneration

Desorption

Desorption is one of the important properties of adsorbents because it relates closely to the scalability of materials in practice (Luo et al. 2021). In contrast with the adsorption process, chloramphenicol molecules are released back from or through the surface of the adsorbent during desorption Yang et al. (2020a, b). In general, the efficiency of chloramphenicol desorption is highly dependent on the eluents. Based on Table 8, the solutions to elute chloramphenicol from the adsorbent can be divided into two categories involving organic eluents, e.g., methanol, and ethanol, and inorganic eluents, e.g., sodium hydroxide, and potassium hydroxide. For organic eluents, Ahmed et al. (2017c) used methanol as an efficient eluent for the desorption of chloramphenicol loaded on ortho-phosphoric acid-functionalized biochar. Indeed, this solvent can desorb 91%, 86%, and 89.2% of chloramphenicol from deionized water, synthetic wastewater, and lake water, respectively. For organic eluents, Li et al. (2018) compared the chloramphenicol desorption efficiency using various eluents such as 0.1 M NaOH, 95% ethanol, 1.0 M NaCl, 0.01 M NaCl, and distilled water. The results indicated that chloramphenicol could be desorbed best up to 58.1% from *Typha orientalis*-derived activated carbon using 0.1 M NaOH. To improve the elution efficiency, Ahammad et al. (2021) insightfully investigated the parameters affecting the desorption of chloramphenicol and selected the best eluent among water, ethanol, and NaCl. The authors found the strong effect of initial concentration and operating temperature on desorption efficiency. Accordingly, 0.8 M NaCl was also suggested as the most appropriate solvent to desorb 84.7% of chloramphenicol from alginate beads-derived ordered mesoporous carbon. Another advantage of using an aqueous NaCl solution might be its inexpensiveness and safety compared with ethanol.

Regeneration

In general, reusable adsorbents boost economic efficiency, sustainability, as well as industrial-scale project development (Ahammad et al. 2021). The regeneration study is to demonstrate the life cycle of adsorbents as well as their stability (Zhao et al. 2020). According to Table 8, the regeneration number of almost adsorbents after the treatment of chloramphenicol is at least four cycles. Besides, the difference in chloramphenicol adsorption capacity between the first and last time is mostly below 20% for various adsorbents. In particular, Dai et al. (2018b) evidenced that the magnetic hierarchical porous carbon obtained an excellent reusability up to twenty times with an insignificant decrease of 18.9% in adsorption capacity in the last cycle. Tran et al. (2019a, b, c) suggested that a mixture of methanol and acetic acid with a respective volume ratio of 9:1 was the most suitable eluent for desorbing chloramphenicol from mesoporous carbon produced by pyrolysis of metal–organic framework $Fe_3O(BDC)_3$, BDC: benzene–1,4–dicarboxylate. Indeed, the results indicated that chloramphenicol adsorption capacity of this adsorbent in the first time was 41.0 mg g^{-1}, compared with 34.7 mg g^{-1} of the fourth time, a minor decrease of around 15%. With the same mixed solvent system, Ma et al. (2020) reported that the chloramphenicol adsorption efficiency of porous molecularly imprinted polymers was inconsiderably declined by 11.42% after the eighth elution. In another work, Tian et al. (2017) showed that potassium citrate-activated–porous carbons were highly regenerative with five times during chloramphenicol treatment. Specifically, sodium hydroxide at a concentration of 0.2 M was suitable for desorbing chloramphenicol from the adsorbent. A negligible decrease in chloramphenicol adsorption capacity from 490 mg g^{-1} to 457 mg g^{-1} was observed after fifth reuse. In summary, mentioned adsorbents offered good stability and reusability performance. However, future studies should specifically address the handling of eluents after reuse to better understand their environmental impacts.

Perspective

The state-of-the-art technologies for antibiotics treatment from wastewater can encounter a number of potential obstacles and constraints. To fulfill the purposes of sustainable development, analysis and assessment of knowledge gaps are required. *Firstly*, comprehensive assessments on the specific toxicity of adsorbent materials during the decontamination of chloramphenicol in water are restricted. Numerous adsorbents can be degraded into hazardous compounds, leading secondary pollution. *Secondly*, various beneficial indicators, such as chemical oxygen demand and biochemical oxygen demand, providing the information on water quality after chloramphenicol treatment should be examined. *Thirdly*, most studies documented the treatment of chloramphenicol on a laboratory scale, without large-scale or pilot surveys. Considering the practicalities of eliminating chloramphenicol and other antibiotic contaminants by scale-up process needs to be discussed. *Fourth,* the remediation of utilized adsorbents receives little post-adsorption attention. Inappropriate disposal of these used materials results in the

Table 8 Chloramphenicol desorption and recyclability of various adsorbents. Note that DE: desorption efficiency, RE: removal efficiency, 1st cycle: first cycle, nth cycle: nth cycle, Q_m: maximum adsorption capacity, [a] data estimated from the figures of the referred study

Adsorbent	Eluent	DE (%)	RE (%)		Q_m (mg g^{-1})		Cycle number	References
			1st cycle	nth cycle	1st cycle	nth cycle		
H_3PO_4-activated biochar at 600 °C	Methanol	91.0	97 [a]	100 [a]			6	Ahmed et al. (2017b)
Typha orientalis-based activated carbon	0.1 M NaOH	58.1	–	–	–	–	–	Li et al. (2018)
Ordered mesoporous carbon–alginate beads	0.8 M NaCl	84.7	76.02	35.20	–	–	5	Ahammad et al. (2021)
Potassium citrate-activated porous carbons at 900 °C	0.1 M KOH	–	–	–	550 [a]	486,29 [a]	5	Dai et al. (2018c)
Porous carbons from potassium citrate pyrolyzed at 850 °C	0.2 M NaOH	–	–	–	490 [a]	457 [a]	5	Tian et al. (2017)
Bovine bone-based hierarchical porous carbon	1% KOH aqueous solution	–	92 [a]	82 [a]	–	–	4	Dai et al. (2018a)
Hierarchical porous carbons from sodium carboxymethyl cellulose	0.2 M NaOH	–	–	–	685 [a]	559.8	5	Zhang et al. (2017)
Shrimp shell-based hierarchical porous carbons	0.2 M NaOH	–	95 [a]	83 [a]	–	–	3	Qin et al. (2016)
Magnetic amine-doped hierarchical porous carbon	0.2 M KOH	–	–	–	445 [a]	360 [a]	20	Dai et al. (2018b)
Peanut shell-based porous biochar	Methanol	–	95 [a]	91 [a]	–	–	4	Yang et al. (2020a, b)
Core–shell molecularly imprinted polymers based on magnetic chitosan	Methanol/acetic acid (9:1)	–	–	–	12.76 [a]	12.02 [a]	8	Ma et al. (2015)
Porous molecularly imprinted polymer halloysite nanotube	Methanol/acetic acid (9:1)	–	–	–	17.77 [a]	15.74 [a]	8	Ma et al. (2020)
Core–shell surface imprinted nanospheres–magnetic mesoporous nanosilica	Methanol and acetic acid (9:1)	–	–	–	10.8	9.98	6	Dai et al. (2016)
Fe_3O_4-supported bovine serum albumin	Ethanol	–	97 [a]	96 [a]	–	–	6	Zhang et al. (2013)
Porous carbon from $Cu_3(BTC)_2$ pyrolyzed at 700 °C	Methanol/acetic acid (9:1)	–	–	–	41	34.7	4	Tran et al. (2019a, b, c)
Nanoscale zero-valent iron particles supported activated carbon	Alcohol	–	–	–	545.25	33.665	4	Wu et al. (2018)

leakage of chloramphenicol contaminants into the aquatic system. *Fifthly*, decontamination of chloramphenicol in the presence of other impurities such as antibiotics, dyes, metal ions, inorganic and organic compounds should be evaluated extensively. This emphasizes the significance of simultaneous removal in achieving practical water purification. *Sixthly*, the evaluation of economic aspects of the total chloramphenicol treatment process has not been explicitly addressed in prior studies. The expense of adsorbents is worth considering since it is one of the leading

selection factors to tackle the chloramphenicol pollution issue. To sum up, these are inherent shortcomings that previous researches have still confronted.

In terms of perspective aspects, design and development of innovative adsorbents are auspicious for environmental remediation against chloramphenicol and other antibiotic contaminants. Adsorbents have been implemented to ensure large specific pore and surface areas, e.g., porous carbon, composites, metal–organic frameworks, and polymers with high adsorption efficiency for chloramphenicol. In particular, the advancement of adsorbents originated from wastes and biomass, e.g., agricultural wastes, floral wastes, food wastes, grape sludge, and shrimp shells as value-added products has lately contributed greatly to tackling such both pollution threats. These immense potentials not only save production costs but also improve antibiotic adsorption performance. It is therefore important to conduct more investigations of taking advantage of wastes as raw materials for adsorbent production. Moreover, several recommendations for enhancing chloramphenicol treatment efficiency while reusing adsorbents can be offered. For example, to maximize the total removal efficiency, integrated strategies including adsorption-catalysis, adsorption-membrane, adsorption-oxidation, adsorption-ionic exchange should be considered. To mitigate the used adsorbents, some post-treatment technologies such as impregnation in fast-setting polymers, concrete mixes, and geopolymerisation in alumina-silicates, and so forth can be employed, but they must be evaluated initially. Eventually, it is necessary to issue precise regulations governing the use of chloramphenicol and other antibiotics in the communities.

Conclusion

Summarily, we provided a comprehensive overview of contamination, toxicity, treatment techniques of chloramphenicol in aquatic environments. The distribution of chloramphenicol is typically centered in the rivers in developing countries. The toxicity of chloramphenicol to creatures and humans has been evaluated. Carbon-based adsorbents were revealed as promising materials to adsorb chloramphenicol. Among the influential factors, pH played a key role in regulating chloramphenicol adsorption. Electron–donor–acceptor was the most prevalent mechanism for chloramphenicol adsorption. Langmuir and pseudo-second-order models were best fitted with the adsorption process. Among eluents, NaOH and methanol were the most commonly utilized solvents for desorbing chloramphenicol from adsorbents. Almost all materials were reported having high recyclability, at least 4 cycles. This review is anticipated to pave the way for the synthesis of benign novel adsorbents for eliminating antibiotics from water.

Acknowledgements The authors would love to appreciate the effort of researchers all over the world in the fight against the COVID-19 pandemic. We also acknowledge Mina Rees Library, The Graduate Center of the City University of New York (CUNY) for granting access to databases, Freepik company projects at www.freepik.com, and Canva® graphic design platforms at www.canva.com for many graphic resources reproduced in this work.

Authors contributions L.M.N. was involved in investigation; data curation; validation; writing—original draft. N.T.T.N. contributed to data curation; investigation; methodology. T.T.T.N. and T.T.N. contributed to data curation; validation. D.T.C.N. and T.V.T. were involved in conceptualization; writing—review and editing; validation; data curation; supervision; English editing; project administration. All authors read and approved the final manuscript.

Availability of data and material The authors declare that all data and materials support their published claims and comply with field standards.

Code availability The authors declare that software application or custom code supports their published claims and complies with field standards.

Declarations

Conflict of interest The authors declare that there are no conflict of interest.

References

Abbasi AR, Rizvandi M (2018) Influence of the ultrasound-assisted synthesis of Cu–BTC metal–organic frameworks nanoparticles on uptake and release properties of rifampicin. Ultrason Sonochem 40:465–471. https://doi.org/10.1016/j.ultsonch.2017.07.041

Ahammad NA, Zulkifli MA, Ahmad MA, Hameed BH, Din ATM (2021) Desorption of chloramphenicol from ordered mesoporous carbon-alginate beads: effects of operating parameters, and isotherm, kinetics, and regeneration studies. J Environ Chem Eng 9:105015

Ahmed MB, Zhou JL, Ngo HH, Guo W, Johir MAH, Belhaj D (2017a) Competitive sorption affinity of sulfonamides and chloramphenicol antibiotics toward functionalized biochar for water and wastewater treatment. Bioresour Technol 238:306–312

Ahmed MB, Zhou JL, Ngo HH, Guo W, Johir MAH, Sornalingam K, Belhaj D, Kallel M (2017b) Nano-Fe0 immobilized onto functionalized biochar gaining excellent stability during sorption and reduction of chloramphenicol via transforming to reusable magnetic composite. Chem Eng J 322:571–581

Ahmed MB, Zhou JL, Ngo HH, Guo W, Johir MAH, Sornalingam K, Rahman MS (2017c) Chloramphenicol interaction with functionalized biochar in water: sorptive mechanism, molecular imprinting effect and repeatable application. Sci Total Environ 609:885–895

Ali N, Zaman H, Bilal M, Shah A-HA, Nazir MS, Iqbal HMN (2019) Environmental perspectives of interfacially active and

magnetically recoverable composite materials—a review. Sci Total Environ 670:523–538. https://doi.org/10.1016/j.scitotenv.2019.03.209

Ambekar CS, Cheung B, Lee J, Chan LC, Liang R, Kumana CR (2000) Metabolism of chloramphenicol succinate in human bone marrow. Eur J Clin Pharmacol 1:405–409. https://doi.org/10.1007/S002280000143

Balarak D, Khatibi AD, Chandrika K (2020) Antibiotics removal from aqueous Solution and pharmaceutical wastewater by adsorption process: a review. Int J Pharm Investig 10:106–111

Bayrakci M, Keskinates M, Yilmaz B (2021) Antibacterial, thermal decomposition and in vitro time release studies of chloramphenicol from novel PLA and PVA nanofiber mats. Mater Sci Eng C 122:111895. https://doi.org/10.1016/j.msec.2021.111895

Bi Z, Kong Q, Cao Y, Sun G, Su F, Wei X, Li X, Ahmad A, Xie L, Chen C-M (2019) Biomass-derived porous carbon materials with different dimensions for supercapacitor electrodes: a review. J Mater Chem A 7:16028–16045

Busch G, Kassas B, Palma MA, Risius A (2020) Perceptions of antibiotic use in livestock farming in Germany, Italy and the United States. Livest Sci 241:104251. https://doi.org/10.1016/j.livsci.2020.104251

Campa-Córdova AI, Luna-González A, Ascencio F, Cortés-Jacinto E, Cáceres-Martínez CJ (2006) Effects of chloramphenicol, erythromycin, and furazolidone on growth of Isochrysis galbana and Chaetoceros gracilis. Aquaculture 260:145–150. https://doi.org/10.1016/j.aquaculture.2006.06.014

Cao Y, Qiu W, Zhao Y, Li J, Jiang J, Yang Y, Pang S-Y, Liu G (2020) The degradation of chloramphenicol by O3/PMS and the impact of O3-based AOPs pre-oxidation on dichloroacetamide generation in post-chlorination. Chem Eng J 401:126146. https://doi.org/10.1016/j.cej.2020.126146

Carrales-Alvarado DH, Leyva-Ramos R, Rodríguez-Ramos I, Mendoza-Mendoza E, Moral-Rodríguez AE (2020) Adsorption capacity of different types of carbon nanotubes towards metronidazole and dimetridazole antibiotics from aqueous solutions: effect of morphology and surface chemistry. Environ Sci Pollut Res 27:17123–17137. https://doi.org/10.1007/s11356-020-08110-x

Chaturvedi P, Shukla P, Giri BS, Chowdhary P, Chandra R, Gupta P, Pandey A (2021) Prevalence and hazardous impact of pharmaceutical and personal care products and antibiotics in environment: a review on emerging contaminants. Environ Res 194:110664. https://doi.org/10.1016/j.envres.2020.110664

Chen A, Pang J, Wei X, Chen B, Xie Y (2021) Fast one-step preparation of porous carbon with hierarchical oxygen-enriched structure from waste lignin for chloramphenicol removal. Environ Sci Pollut Res 28:27398–27410

Chen D, Delmas J-M, Hurtaud-Pessel D, Verdon E (2020a) Development of a multi-class method to determine nitroimidazoles, nitrofurans, pharmacologically active dyes and chloramphenicol in aquaculture products by liquid chromatography-tandem mass spectrometry. Food Chem 311:125924. https://doi.org/10.1016/j.foodchem.2019.125924

Chen S, Hu J, Han S, Guo Y, Belzile N, Deng T (2020b) A review on emerging composite materials for cesium adsorption and environmental remediation on the latest decade. Sep Purif Technol 251:117340

Cheng D, Ngo HH, Guo W, Chang SW, Nguyen DD, Liu Y, Wei Q, Wei D (2020) A critical review on antibiotics and hormones in swine wastewater: water pollution problems and control approaches. J Hazard Mater 387:121682. https://doi.org/10.1016/j.jhazmat.2019.121682

Cheng N, Wang B, Wu P, Lee X, Xing Y, Chen M, Gao B (2021) Adsorption of emerging contaminants from water and wastewater by modified biochar: a review. Environ Pollut 1:116448

Cheng X, Zheng C, Lu Q, Liu J, Wang Q, Fan Y, Zhang J (2019) Adsorption of Furazolidone, D-Cycloserine, and Chloramphenicol on Granular Activated Carbon Made from Corn Stover. J Environ Eng 145:04019038. https://doi.org/10.1061/(ASCE)EE.1943-7870.0001546

Chitongo R, Opeolu BO, Olatunji OS (2019) Abatement of amoxicillin, ampicillin, and chloramphenicol from aqueous solutions using activated carbon prepared from grape slurry. CLEAN–Soil Air Water 47:1877.

Choi K, Kim Y, Jung J, Kim MH, Kim CS, Kim NH, Park J (2008) Occurrences and ecological risks of roxithromycin, trimethoprim, and chloramphenicol in the Han River, Korea. Environ Toxicol Chem 27:711–719. https://doi.org/10.1897/07-143.1

Christensen LK, Skovsted L (1969) Inhibition of drug metabolism by chloramphenicol. Lancet 2:1397–1399. https://doi.org/10.1016/S0140-6736(69)90937-4

Cuerda-Correa EM, Alexandre-Franco MF, Fernández-González C (2020) Advanced oxidation processes for the removal of antibiotics from water. An overview. Water https://doi.org/10.3390/w12010102

Dai J, He J, Xie A, Gao L, Pan J, Chen X, Zhou Z, Wei X, Yan Y (2016) Novel pitaya-inspired well-defined core–shell nanospheres with ultrathin surface imprinted nanofilm from magnetic mesoporous nanosilica for highly efficient chloramphenicol removal. Chem Eng J 284:812–822. https://doi.org/10.1016/j.cej.2015.09.050

Dai J, Qin L, Zhang R, Xie A, Chang Z, Tian S, Li C, Yan Y (2018a) Sustainable bovine bone-derived hierarchically porous carbons with excellent adsorption of antibiotics: equilibrium, kinetic and thermodynamic investigation. Powder Technol 331:162–170

Dai J, Tian S, Jiang Y, Chang Z, Xie A, Zhang R, Li C, Yan Y (2018b) Fe3C/Fe/C magnetic hierarchical porous carbon with micromesopores for highly efficient chloramphenicol adsorption: magnetization, graphitization, and adsorption properties investigation. Ind Eng Chem Res 57:3510–3522

Dai J, Tian S, Jiang Y, Chang Z, Xie A, Zhang R, Yan Y (2018c) Facile synthesis of porous carbon sheets from potassium acetate via in-situ template and self-activation for highly efficient chloramphenicol removal. J Alloys Compd 732:222–232

Dai Y, Zhang N, Xing C, Cui Q, Sun Q (2019) The adsorption, regeneration and engineering applications of biochar for removal organic pollutants: a review. Chemosphere 223:12–27

Deng H, Doonan CJ, Furukawa H, Ferreira RB, Towne J, Knobler CB, Wang B, Yaghi OM (2010) Multiple functional groups of varying ratios in metal-organic frameworks. Science 327:846–850

Dissanayake Herath GA, Poh LS, Ng WJ (2019) Statistical optimization of glyphosate adsorption by biochar and activated carbon with response surface methodology. Chemosphere 227:533–540. https://doi.org/10.1016/j.chemosphere.2019.04.078

Dowling PM (2013) Antimicrobial therapy in veterinary medicine, antimicrobial therapy in veterinary medicine. Wiley. https://doi.org/10.1002/9781118675014

Dutt MA, Hanif MA, Nadeem F, Bhatti HN (2020) A review of advances in engineered composite materials popular for wastewater treatment. J Environ Chem Eng 8:1073. https://doi.org/10.1016/j.jece.2020.104073

Fan Y, Wang B, Yuan S, Wu X, Chen J, Wang L (2010) Adsorptive removal of chloramphenicol from wastewater by NaOH modified bamboo charcoal. Bioresour Technol 101:7661–7664

Fresco-Cala B, Batista AD, Cárdenas S (2020) Molecularly imprinted polymer micro-and nano-particles: a review. Molecules 25:4740

Geng X, Lv S, Yang J, Cui S, Zhao Z (2021) Carboxyl-functionalized biochar derived from walnut shells with enhanced aqueous adsorption of sulfonamide antibiotics. J Environ Manag 280:111749. https://doi.org/10.1016/j.jenvman.2020.111749

Gopal CM, Bhat K, Ramaswamy BR, Kumar V, Singhal RK, Basu H, Udayashankar HN, Vasantharaju SG, Praveenkumarreddy

Y, Shailesh L, Y., Balakrishna, K., (2021) Seasonal occurrence and risk assessment of pharmaceutical and personal care products in Bengaluru rivers and lakes, India. J Environ Chem Eng 9:105610. https://doi.org/10.1016/j.jece.2021.105610

Gu X, Xu Z, Gu L, Xu H, Han F, Chen B, Pan X (2021) Preparation and antibacterial properties of gold nanoparticles: a review. Environ Chem Lett 19:167–187. https://doi.org/10.1007/s10311-020-01071-0

Holanda FH, e, Birolli, W.G., Morais, E. dos S., Sena, I.S., Ferreira, A.M., Faustino, S.M.M., Grace da S. Solon, L., Porto, A.L.M., Ferreira, I.M., (2019) Study of biodegradation of chloramphenicol by endophytic fungi isolated from Bertholletia excelsa (Brazil nuts). Biocatal Agric Biotechnol 20:101200. https://doi.org/10.1016/j.bcab.2019.101200

Huys G, Bartie K, Cnockaert M, Hoang Oanh DT, Phuong NT, Somsiri T, Chinabut S, Yusoff FM, Shariff M, Giacomini M, Teale A, Swings J (2007) Biodiversity of chloramphenicol-resistant mesophilic heterotrophs from Southeast Asian aquaculture environments. Res Microbiol 158:228–235. https://doi.org/10.1016/j.resmic.2006.12.011

Idris ZM, Hameed BH, Ye L, Hajizadeh S, Mattiasson B, Din ATM (2020) Amino-functionalised silica-grafted molecularly imprinted polymers for chloramphenicol adsorption. J Environ Chem Eng 8:103981

Jiang L, Hu X, Yin D, Zhang H, Yu Z (2011) Occurrence, distribution and seasonal variation of antibiotics in the Huangpu River, Shanghai, China. Chemosphere 82:822–828. https://doi.org/10.1016/j.chemosphere.2010.11.028

Kaparapu J (2018) Application of microalgae in aquaculture. Phykos 48:21–26

Kasprzyk-Hordern B, Dinsdale RM, Guwy AJ (2009) The removal of pharmaceuticals, personal care products, endocrine disruptors and illicit drugs during wastewater treatment and its impact on the quality of receiving waters. Water Res 43:363–380. https://doi.org/10.1016/j.watres.2008.10.047

Kimosop SJ, Getenga ZM, Orata F, Okello VA, Cheruiyot JK (2016) Residue levels and discharge loads of antibiotics in wastewater treatment plants (WWTPs), hospital lagoons, and rivers within Lake Victoria Basin, Kenya. Environ Monit Assess. https://doi.org/10.1007/S10661-016-5534-6

Klebaniuk R, Tomaszewska E, Dobrowolski P, Kwiecień M, Burmańczuk A, Yanovych D, Zasadna Z, Szymańczyk S, Burmańczuk N, Muszyński S (2018) Chloramphenicol-induced alterations in the liver and small intestine epithelium in pigs. Anim Sci 18:429–440. https://doi.org/10.2478/aoas-2018-0001

Kong D, Liang B, Lee D-J, Wang A, Ren N (2014) Effect of temperature switchover on the degradation of antibiotic chloramphenicol by biocathode bioelectrochemical system. J Environ Sci 26:1689–1697. https://doi.org/10.1016/j.jes.2014.06.009

Koup JR, Gibaldi M, McNamara P, Hilligoss DM, Colburn WA, Bruck E (1978) Interaction of chloramphenicol with phenytoin and phenobarbital; Case report. Clin Pharmacol Ther 24:571–575. https://doi.org/10.1002/cpt1978245571

Kumar A, Sharma K, Dixit AR (2020) Carbon nanotube- and graphene-reinforced multiphase polymeric composites: review on their properties and applications. J Mater Sci 55:2682–2724. https://doi.org/10.1007/s10853-019-04196-y

Lach J (2019) Adsorption of chloramphenicol on commercial and modified activated carbons. Water (switzerland). https://doi.org/10.3390/W11061141

Lach J, Ociepa-Kubicka A (2017) The removal of chloramphenicol from water through adsorption on activated carbon. E3S Web Conf 19:02008. https://doi.org/10.1051/e3sconf/20171902008

Lai HT, Hou JH, Su CI, Chen CL (2009) Effects of chloramphenicol, florfenicol, and thiamphenicol on growth of algae Chlorella pyrenoidosa, Isochrysis galbana, and Tetraselmis chui. Ecotoxicol Environ Saf 72:329–334. https://doi.org/10.1016/j.ecoenv.2008.03.005

Leston S, Nunes M, Viegas I, Ramos F, Pardal MÂ (2013) The effects of chloramphenicol on Ulva lactuca. Chemosphere 91:552–557

Li A, Zhou M, Luo P, Shang J, Wang P, Lyu L (2020a) Deposition of MOFs on polydopamine-modified electrospun polyvinyl alcohol/silica nanofibers mats for chloramphenicol adsorption in water. NANO 15:2050046. https://doi.org/10.1142/S1793292020500460

Li N, Zhou L, Jin X, Owens G, Chen Z (2019) Simultaneous removal of tetracycline and oxytetracycline antibiotics from wastewater using a ZIF-8 metal organic-framework. J Hazard Mater 366:563–572. https://doi.org/10.1016/j.jhazmat.2018.12.047

Li P, Wu Y, He Y, Zhang B, Huang Y, Yuan Q, Chen Y (2020b) Occurrence and fate of antibiotic residues and antibiotic resistance genes in a reservoir with ecological purification facilities for drinking water sources. Sci Total Environ 707:135276. https://doi.org/10.1016/j.scitotenv.2019.135276

Li X, Yang X, Xue H, Pang H, Xu Q (2020c) Metal–organic frameworks as a platform for clean energy applications. EnergyChem 2:100027

Li Y, Zhang J, Liu H (2018) Removal of chloramphenicol from aqueous solution using low-cost activated carbon prepared from Typha orientalis. Water 10:351

Li Y, Zhao H-P, Zhu L (2021) Remediation of soil contaminated with organic compounds by nanoscale zero-valent iron: A review. Sci Total Environ 760:1413

Li Z, Sun Y, Yang Y, Han Y, Wang T, Chen J, Tsang DCW (2020d) Biochar-supported nanoscale zero-valent iron as an efficient catalyst for organic degradation in groundwater. J Hazard Mater 383:121240. https://doi.org/10.1016/j.jhazmat.2019.121240

Liao P, Zhan Z, Dai J, Wu X, Zhang W, Wang K, Yuan S (2013) Adsorption of tetracycline and chloramphenicol in aqueous solutions by bamboo charcoal: a batch and fixed-bed column study. Chem Eng J 228:496–505

Lima EC, Sher F, Guleria A, Saeb MR, Anastopoulos I, Tran HN, Hosseini-Bandegharaei A (2021) Is one performing the treatment data of adsorption kinetics correctly? J Environ Chem Eng 9:104813. https://doi.org/10.1016/j.jece.2020.104813

Lin AY-C, Yu T-H, Lin C-F (2008) Pharmaceutical contamination in residential, industrial, and agricultural waste streams: risk to aqueous environments in Taiwan. Chemosphere 74:131–141. https://doi.org/10.1016/j.chemosphere.2008.08.027

Liu H, Lv Y, Zhang Y-N, Zhang Y, Qu J, Dong D, Wang Z, Hua X (2021) Effective electrocatalytic elimination of chloramphenicol: Mechanism, degradation pathway, and toxicity assessment. Environ Sci Pollut Res 28:67843–67851. https://doi.org/10.1007/s11356-021-15403-2

Liu H, Zhang G, Liu C-Q, Li L, Xiang M (2009) The occurrence of chloramphenicol and tetracyclines in municipal sewage and the Nanming River, Guiyang City, China. J Environ Monit 11:1199. https://doi.org/10.1039/b820492f

Liu X, Wang Y (2019) Activated carbon supported nanoscale zero-valent iron composite: aspects of surface structure and composition. Mater Chem Phys 222:369–376

Lu XW, Dang Z, Yang C (2009) Preliminary investigation of chloramphenicol in fish, water and sediment from freshwater aquaculture pond. Int J Environ Sci Technol 6:597–604

Lu Z-Y, Ma Y-L, Zhang J-T, Fan N-S, Huang B-C, Jin R-C (2020) A critical review of antibiotic removal strategies: performance and mechanisms. J Water Process Eng 38:101681

Lulijwa R, Rupia EJ, Alfaro AC (2020) Antibiotic use in aquaculture, policies and regulation, health and environmental risks: a review of the top 15 major producers. Rev Aquac 12:640–663

Luo B, Huang G, Yao Y, An C, Zhang P, Zhao K (2021) Investigation into the influencing factors and adsorption characteristics in the removal of sulfonamide antibiotics by carbonaceous materials. J Clean Prod 319:128692. https://doi.org/10.1016/j.jclepro.2021.128692

Luo L, Gu C, Li M, Zheng X, Zheng F (2018) Determination of residual 4-nitrobenzaldehyde in chloramphenicol and its pharmaceutical formulation by HPLC with UV/Vis detection after derivatization with 3-nitrophenylhydrazine. J Pharm Biomed Anal 156:307–312. https://doi.org/10.1016/j.jpba.2018.04.024

Lv Z, Yang S, Chen L, Alsaedi A, Hayat T, Chen C (2019) Nanoscale zero-valent iron/magnetite carbon composites for highly efficient immobilization of U (VI). J Environ Sci 76:377–387

Ma W, Dai J, Dai X, Da Z, Yan Y (2015) Core–shell molecularly imprinted polymers based on magnetic chitosan microspheres for chloramphenicol selective adsorption. Monatshefte Für Chemie - Chem Mon 146:465–474

Ma Y, Dai J, Wang L, Yan Y, Gao M (2020) Fabrication of porous molecularly imprinted polymer using halloysite nanotube as template for selective recognition and separation of chloramphenicol. J Iran Chem Soc 17:555–565

Mahdi MH, Mohammed TJ, Al-Najar JA (2021) Advanced Oxidation Processes (AOPs) for treatment of antibiotics in wastewater: a review. In: IOP Conference Series: Earth and Environmental Science. IOP Publishing, p 12109

Masoomi MY, Bagheri M, Morsali A (2017) Porosity and dye adsorption enhancement by ultrasonic synthesized Cd(II) based metal-organic framework. Ultrason Sonochem 37:244–250. https://doi.org/10.1016/j.ultsonch.2017.01.018

McIntyre J, Choonara I (2004) Drug toxicity in the neonate. Neonatology 86:218–221. https://doi.org/10.1159/000079656

Minh TB, Leung HW, Loi IH, Chan WH, So MK, Mao JQ, Choi D, Lam JCW, Zheng G, Martin M, Lee JHW, Lam PKS, Richardson BJ (2009) Antibiotics in the Hong Kong metropolitan area: ubiquitous distribution and fate in Victoria Harbour. Mar Pollut Bull 58:1052–1062. https://doi.org/10.1016/j.marpolbul.2009.02.004

Mohd Din AT, Ahmad MA, Hameed BH (2015) Ordered mesoporous carbons originated from non-edible polyethylene glycol 400 (PEG-400) for chloramphenicol antibiotic recovery from liquid phase. Chem Eng J 260:730–739. https://doi.org/10.1016/j.cej.2014.09.010

Nasseh N, Barikbin B, Taghavi L, Nasseri MA (2019) Adsorption of metronidazole antibiotic using a new magnetic nanocomposite from simulated wastewater (isotherm, kinetic and thermodynamic studies). Compos Part B Eng 159:146–156. https://doi.org/10.1016/j.compositesb.2018.09.034

Ngo HH, Guo W, Ton-That C, Li J, Li J, Liu Y (2017) Removal of antibiotics (sulfamethazine, tetracycline and chloramphenicol) from aqueous solution by raw and nitrogen plasma modified steel shavings. Sci Total Environ 601:845–856

Oberoi AS, Jia Y, Zhang H, Khanal SK, Lu H (2019) Insights into the fate and removal of antibiotics in engineered biological treatment systems: a critical review. Environ Sci Technol 53:7234–7264. https://doi.org/10.1021/acs.est.9b01131

Ohnishi S, Murata M, Ida N, Oikawa S, Kawanishi S (2015) Oxidative DNA damage induced by metabolites of chloramphenicol, an antibiotic drug. Free Radic Res 49:1165–1172. https://doi.org/10.3109/10715762.2015.1050963

Oluwatosin O, Adekunle B, Obih U, Arne H (2016) Quantification of pharmaceutical residues in wastewater impacted surface waters and sewage sludge from Lagos, Nigeria. J Environ Chem Ecotoxicol 8:14–24. https://doi.org/10.5897/JECE2015.0364

Ouyang J, Zhou L, Liu Z, Heng JYY, Chen W (2020) Biomass-derived activated carbons for the removal of pharmaceutical mircopollutants from wastewater: A review. Sep Purif Technol 253:117536

Parthasarathy R, Chandrika M, Yashavantha Rao HC, Kamalraj S, Jayabaskaran C, Pugazhendhi A (2020) Molecular profiling of marine endophytic fungi from green algae: Assessment of antibacterial and anticancer activities. Process Biochem 96:11–20. https://doi.org/10.1016/j.procbio.2020.05.012

Peng X, Wang Z, Kuang W, Tan J, Li K (2006) A preliminary study on the occurrence and behavior of sulfonamides, ofloxacin and chloramphenicol antimicrobials in wastewaters of two sewage treatment plants in Guangzhou. China Sci Total Environ 371:314–322. https://doi.org/10.1016/j.scitotenv.2006.07.001

Penny RH, Carlisle CH, Prescott CW, Davidson HA (1967) Effects of chloramphenicol on the haemopoietic system of the cat. Br Vet J 123:145–152. https://doi.org/10.1016/S0007-1935(17)40053-4

Praveena SM, Shaifuddin SNM, Sukiman S, Nasir FAM, Hanafi Z, Kamarudin N, Ismail THT, Aris AZ (2018) Pharmaceuticals residues in selected tropical surface water bodies from Selangor (Malaysia): occurrence and potential risk assessments. Sci Total Environ 642:230–240. https://doi.org/10.1016/j.scitotenv.2018.06.058

Qin L, Liu W, Liu X, Yang Y, Cui C, Zhang L (2020) A review of nano-carbon based molecularly imprinted polymer adsorbents and their adsorptionmechanism. New Carbon Mater 35:459–485

Qin L, Zhou Z, Dai J, Ma P, Zhao H, He J, Xie A, Li C, Yan Y (2016) Novel N-doped hierarchically porous carbons derived from sustainable shrimp shell for high-performance removal of sulfamethazine and chloramphenicol. J Taiwan Inst Chem Eng 62:228–238. https://doi.org/10.1016/j.jtice.2016.02.009

Raju A, Shanmugaraja M (2021) Recent researches in fiber reinforced composite materials: A review. Mater Today Proc 46:9291–9296

Rich ML, Ritterhoff RJ, Hoffmann RJ (1950) A fatal case of aplastic anemia following chloramphenicol (chloromycetin) therapy. Ann Intern Med 33:1459–1467. https://doi.org/10.7326/0003-4819-33-6-1459

Roushani M, Rahmati Z, Farokhi S, Hoseini SJ, Fath RH (2020) The development of an electrochemical nanoaptasensor to sensing chloramphenicol using a nanocomposite consisting of graphene oxide functionalized with (3-Aminopropyl) triethoxysilane and silver nanoparticles. Mater. Sci. Eng. C 108:110388. https://doi.org/10.1016/j.msec.2019.110388

Saba AB, Ola-Davies O, Oyeyemi MO, Ajala O (2016) The toxic effects of prolonged administration of chloramphenicol on the liver and kidney of rats. Afr J Biomed Res 3:133–137. https://doi.org/10.4314/ajbr.v3i3

Safaei M, Foroughi MM, Ebrahimpoor N, Jahani S, Omidi A, Khatami M (2019) A review on metal-organic frameworks: synthesis and applications. TrAC Trends Anal Chem 118:401–425

Sall ML, Diaw AKD, Gningue-Sall D, Efremova Aaron S, Aaron J-J (2020) Toxic heavy metals: impact on the environment and human health, and treatment with conducting organic polymers, a review. Environ Sci Pollut Res 27:29927–29942. https://doi.org/10.1007/s11356-020-09354-3

Samsonova JV, Cannavan A, Elliott CT (2012) A critical review of screening methods for the detection of chloramphenicol, thiamphenicol, and florfenicol residues in foodstuffs. Crit Rev Anal Chem 42:50–78. https://doi.org/10.1080/10408347.2012.629951

Saravanan A, Kumar PS, Vo D-VN, Yaashikaa PR, Karishma S, Jeevanantham S, Gayathri B, Bharathi VD (2021) Photocatalysis for removal of environmental pollutants and fuel production: a review. Environ Chem Lett 19:441–463. https://doi.org/10.1007/s10311-020-01077-8

Shi H, Ni J, Zheng T, Wang X, Wu C, Wang Q (2020) Remediation of wastewater contaminated by antibiotics. A Review Environ Chem Lett 18:345–360

Shukla P, Bansode FW, Singh RK (2011) Chloramphenicol toxicity: a review. J Med Med Sci 2:1313–1316

Simon RD (1973) The effect of chloramphenicol on the production of cyanophycin granule polypeptide in the blue-green alga Anabaena cylindrica. Arch Mikrobiol 92:115–122. https://doi.org/10.1007/BF00425009

Stevenson J (2014) Ecological assessments with algae: a review and synthesis. J Phycol 50:437–461

Sui Q, Huang J, Deng S, Chen W, Yu G (2011) Seasonal variation in the occurrence and removal of pharmaceuticals and personal care products in different biological wastewater treatment processes. Environ Sci Technol 45:3341–3348. https://doi.org/10.1021/es200248d

Sui Q, Huang J, Deng S, Yu G, Fan Q (2010) Occurrence and removal of pharmaceuticals, caffeine and DEET in wastewater treatment plants of Beijing, China. Water Res 44:417–426. https://doi.org/10.1016/j.watres.2009.07.010

Sun K, Shi Y, Xu W, Potter N, Li Z, Zhu J (2017) Modification of clays and zeolites by ionic liquids for the uptake of chloramphenicol from water. Chem Eng J 313:336–344

Tahrani L, Van Loco J, Ben Mansour H, Reyns T (2016) Occurrence of antibiotics in pharmaceutical industrial wastewater, wastewater treatment plant and sea waters in Tunisia. J Water Health 14:208–213. https://doi.org/10.2166/wh.2015.224

Tian S, Dai J, Jiang Y, Chang Z, Xie A, He J, Zhang R, Yan Y (2017) Facile preparation of intercrossed-stacked porous carbon originated from potassium citrate and their highly effective adsorption performance for chloramphenicol. J Colloid Interface Sci 505:858–869

Tong L, Li P, Wang Y, Zhu K (2009) Analysis of veterinary antibiotic residues in swine wastewater and environmental water samples using optimized SPE-LC/MS/MS. Chemosphere 74:1090–1097. https://doi.org/10.1016/j.chemosphere.2008.10.051

Tong Y, McNamara PJ, Mayer BK (2019) Adsorption of organic micropollutants onto biochar: a review of relevant kinetics, mechanisms and equilibrium. Environ Sci Water Res Technol 5:821–838

Tran NH, Chen H, Reinhard M, Mao F, Gin KY-H (2016) Occurrence and removal of multiple classes of antibiotics and antimicrobial agents in biological wastewater treatment processes. Water Res 104:461–472. https://doi.org/10.1016/j.watres.2016.08.040

Tran NH, Hoang L, Nghiem LD, Nguyen NMH, Ngo HH, Guo W, Trinh QT, Mai NH, Chen H, Nguyen DD (2019a) Occurrence and risk assessment of multiple classes of antibiotics in urban canals and lakes in Hanoi. Vietnam Sci Total Environ 692:157–174

Tran VS, Ngo HH, Guo W, Ton-That C, Li J, Li J, Liu Y (2017) Removal of antibiotics (sulfamethazine, tetracycline and chloramphenicol) from aqueous solution by raw and nitrogen plasma modified steel shavings. Sci Total Environ 601–602:845–856

Tran TV, Nguyen DTC, Le HTN, Bach LG, Vo D-VN, Hong SS, Phan T-QT, Nguyen TD (2019b) Tunable synthesis of mesoporous carbons from Fe3O(BDC)3 for chloramphenicol antibiotic remediation. Nanomaterials 9:237. https://doi.org/10.3390/nano9020237

Tran TV, Nguyen DTC, Le HTN, Ho HL, Nguyen TT, Doan V-D, Nguyen TD, Bach LG (2019c) Response surface methodology-optimized removal of chloramphenicol pharmaceutical from wastewater using Cu3(BTC)2-derived porous carbon as an efficient adsorbent. Comptes Rendus Chim 22:794–803. https://doi.org/10.1016/j.crci.2019.09.004

Tranchemontagne DJ, Mendoza-Cortés JL, O'Keeffe M, Yaghi OM (2009) Secondary building units, nets and bonding in the chemistry of metal–organic frameworks. Chem Soc Rev 38:1257–1283

Turton JA, Fagg R, Sones WR, Williams TC, Andrews CM (2006) Characterization of the myelotoxicity of chloramphenicol succinate in the B6C3F1 mouse. Int J Exp Pathol 87:101–112. https://doi.org/10.1111/J.0959-9673.2006.00460.X

Vaitsis C, Sourkouni G, Argirusis C (2019) Metal organic frameworks (MOFs) and ultrasound: a review. Ultrason Sonochem 52:106–119. https://doi.org/10.1016/j.ultsonch.2018.11.004

Van TTH, Yidana Z, Smooker PM, Coloe PJ (2020) Antibiotic use in food animals worldwide, with a focus on Africa: Pluses and minuses. J Glob Antimicrob Resist 20:170–177. https://doi.org/10.1016/j.jgar.2019.07.031

Wang H, Shan L, Lv Q, Cai S, Quan G, Yan J (2020) Production of hierarchically porous carbon from natural biomass waste for efficient organic contaminants adsorption. J Clean Prod 263:121352.

Wang J, Zhuan R (2020) Degradation of antibiotics by advanced oxidation processes: an overview. Sci Total Environ 701:135023. https://doi.org/10.1016/j.scitotenv.2019.135023

Wang MY, Sadun AA (2013) Drug-related mitochondrial optic neuropathies. J Neuro-Ophthalmology 33:172–178. https://doi.org/10.1097/WNO.0B013E3182901969

Wang X, Xie Y, Tong W, Hu W, Wang Y, Zhang Y (2021) Photochemical degradation of chloramphenicol over jarosite/oxalate system: performance and mechanism investigation. J Environ Chem Eng 9:104570. https://doi.org/10.1016/j.jece.2020.104570

Wang Y, Wang E, Dong H, Liu F, Wu Z, Li H, Wang Y (2014) Synthesis of chitosan-based molecularly imprinted polymers for pre-concentration and clean-up of chloramphenicol. Adsorpt Sci Technol 32:321–330. https://doi.org/10.1260/0263-6174.32.4.321

Watson ADJ (1977) Chloramphenicol toxicity in dogs. Res Vet Sci 23:66–69. https://doi.org/10.1016/S0034-5288(18)33227-2

Wiest DB, Cochran JB, Tecklenburg FW (2012) Chloramphenicol toxicity revisited: a 12-year-old patient with a brain abscess. J Pediatr Pharmacol Ther 17:182–188. https://doi.org/10.5863/1551-6776-17.2.182

Wu Y, Yue Q, Ren Z, Gao B (2018) Immobilization of nanoscale zerovalent iron particles (nZVI) with synthesized activated carbon for the adsorption and degradation of Chloramphenicol (CAP). J Mol Liq 262:19–28. https://doi.org/10.1016/j.molliq.2018.04.032

Xiang Y, Xu Z, Wei Y, Zhou Y, Yang X, Yang Y, Yang J, Zhang J, Luo L, Zhou Z (2019) Carbon-based materials as adsorbent for antibiotics removal: mechanisms and influencing factors. J Environ Manag 237:128–138

Xiang Y, Yang X, Xu Z, Hu W, Zhou Y, Wan Z, Yang Y, Wei Y, Yang J, Tsang DCW (2020) Fabrication of sustainable manganese ferrite modified biochar from vinasse for enhanced adsorption of fluoroquinolone antibiotics: Effects and mechanisms. Sci Total Environ 709:136079. https://doi.org/10.1016/j.scitotenv.2019.136079

Xiong Q, Hu LX, Liu YS, Wang TT, Ying GG (2019) New insight into the toxic effects of chloramphenicol and roxithromycin to algae using FTIR spectroscopy. Aquat Toxicol 207:197–207. https://doi.org/10.1016/j.aquatox.2018.12.017

Xu H, Xiao L, Zheng S, Zhang Y, Li J, Liu F (2019) Reductive degradation of chloramphenicol by Geobacter metallireducens. Sci China Technol Sci 62:1688–1694

Xu J, Liu X, Cao Z, Bai W, Shi Q, Yang Y (2020) Fast degradation, large capacity, and high electron efficiency of chloramphenicol removal by different carbon-supported nanoscale zerovalent iron. J Hazard Mater 384:121253.

Xu L, Zhang H, Xiong P, Zhu Q, Liao C, Jiang G (2021) Occurrence, fate, and risk assessment of typical tetracycline antibiotics in the aquatic environment: a review. Sci Total Environ 753:141975. https://doi.org/10.1016/j.scitotenv.2020.141975

Xu W, hai, Zhang, G., Zou, S. chun, Li, X. dong, Liu, Y. chun, (2007) Determination of selected antibiotics in the Victoria Harbour and the Pearl River, South China using high-performance liquid chromatography-electrospray ionization tandem mass spectrometry.

Environ Pollut 145:672–679. https://doi.org/10.1016/j.envpol.2006.05.038

Yaghi OM, Kalmutzki MJ, Diercks CS (2019) Introduction to reticular chemistry. Mol Front J 4:1

Yang F, Zhang Q, Jian H, Wang C, Xing B, Sun H, Hao Y (2020a) Effect of biochar-derived dissolved organic matter on adsorption of sulfamethoxazole and chloramphenicol. J Hazard Mater. https://doi.org/10.1016/j.jhazmat.2020.122598

Yang J, Ji G, Gao Y, Fu W, Irfan M, Mu L, Zhang Y, Li A (2020b) High-yield and high-performance porous biochar produced from pyrolysis of peanut shell with low-dose ammonium polyphosphate for chloramphenicol adsorption. J Clean Prod. https://doi.org/10.1016/j.jclepro.2020.121516

Yanovych D, Berendsen B, Zasadna Z, Rydchuk M, Czymai T (2018) A study of the origin of chloramphenicol isomers in honey. Drug Test Anal 10:416–422. https://doi.org/10.1002/dta.2234

Yi L, Zuo L, Wei C, Fu H, Qu X, Zheng S, Xu Z, Guo Y, Li H, Zhu D (2020) Enhanced adsorption of bisphenol A, tylosin, and tetracycline from aqueous solution to nitrogen-doped multiwall carbon nanotubes via cation-π and π-π electron-donor-acceptor (EDA) interactions. Sci Total Environ 719:137389. https://doi.org/10.1016/j.scitotenv.2020.137389

Yunis AA (1989) Chloramphenicol toxicity: 25 years of research. Am J Med 87:44N-48N

Zhang B, Zhang H, Li X, Lei X, Li C, Yin D, Fan X, Zhang Q (2013) Synthesis of BSA/Fe3O4 magnetic composite microspheres for adsorption of antibiotics. Mater Sci Eng C 33:4401–4408

Zhang M, Igalavithana AD, Xu L, Sarkar B, Hou D, Zhang M, Bhatnagar A, Cho WC, Ok YS (2021a) Engineered/designer hierarchical porous carbon materials for organic pollutant removal from water and wastewater: a critical review. Crit Rev Environ Sci Technol 51:2295–2328

Zhang R, Zhou Z, Xie A, Dai J, Cui J, Lang J, Wei M, Dai X, Li C, Yan Y (2017) Preparation of hierarchical porous carbons from sodium carboxymethyl cellulose via halloysite template strategy coupled with KOH-activation for efficient removal of chloramphenicol. J Taiwan Inst Chem Eng 80:424–433

Zhang T, Yang Y, Li X, Jiang Y, Fan X, Du P, Li H, Wang N, Zhou Z (2021b) Adsorption characteristics of chloramphenicol onto powdered activated carbon and its desorption performance by ultrasound. Environ Technol (united Kingdom) 42:571–583. https://doi.org/10.1080/09593330.2019.1637464

Zhang Y, Guo P, Wang M, Wu Y, Sun Y, Su H, Deng J (2021c) Mixture toxicity effects of chloramphenicol, thiamphenicol, florfenicol in Daphnia magna under different temperatures. Ecotoxicology 30:31–42. https://doi.org/10.1007/s10646-020-02311-3

Zhang Z, Li X, Zhang C, Lu S, Xi Y, Huang Y, Xue Z, Yang T (2021d) Combining ferrate(VI) with thiosulfate to oxidize chloramphenicol: Influencing factors and degradation mechanism. J Environ Chem Eng 9:104625. https://doi.org/10.1016/j.jece.2020.104625

Zhao H, Liu X, Cao Z, Zhan Y, Shi X, Yang Y, Zhou J, Xu J (2016) Adsorption behavior and mechanism of chloramphenicols, sulfonamides, and non-antibiotic pharmaceuticals on multi-walled carbon nanotubes. J Hazard Mater 310:235–245

Zhao R, Ma T, Zhao S, Rong H, Tian Y, Zhu G (2020) Uniform and stable immobilization of metal-organic frameworks into chitosan matrix for enhanced tetracycline removal from water. Chem Eng J 382:122893. https://doi.org/10.1016/j.cej.2019.122893

Zhao X, Zhao H, Dai W, Wei Y, Wang Y, Zhang Y, Zhi L, Huang H, Gao Z (2018) A metal-organic framework with large 1-D channels and rich OH sites for high-efficiency chloramphenicol removal from water. J Colloid Interface Sci 526:28–34. https://doi.org/10.1016/j.jcis.2018.04.095

Zhou LJ, Li J, Zhang Y, Kong L, Jin M, Yang X, Wu QL (2019) Trends in the occurrence and risk assessment of antibiotics in shallow lakes in the lower-middle reaches of the Yangtze River basin. China Ecotoxicol Environ Saf. https://doi.org/10.1016/j.ecoenv.2019.109511

Zhu X, Gao Y, Yue Q, Kan Y, Kong W, Gao B (2017) Preparation of green alga-based activated carbon with lower impregnation ratio and less activation time by potassium tartrate for adsorption of chloramphenicol. Ecotoxicol Environ Saf 145:289–294. https://doi.org/10.1016/j.ecoenv.2017.07.053

Zhu X, Gao Y, Yue Q, Song Y, Gao B, Xu X (2018) Facile synthesis of hierarchical porous carbon material by potassium tartrate activation for chloramphenicol removal. J Taiwan Inst Chem Eng 85:141–148